J Neurophysiol 101: 1463–1479, 2009.
First published December 17, 2008; doi:10.1152/jn.90681.2008.

Time Course of Cross-Orientation Suppression in the Early Visual Cortex

Rui Kimura[1,2] and Izumi Ohzawa[1,2,3]

[1]*Graduate School of Engineering Science,* [2]*Graduate School of Frontier Biosciences, Osaka University, Toyonaka, Osaka; and* [3]*Core Research for Evolutionary Science and Technology (CREST), Japan Science and Technology Agency, Tokyo, Japan*

Submitted 14 June 2008; accepted in final form 12 December 2008

Kimura R, Ohzawa I. Time course of cross-orientation suppression in the early visual cortex. *J Neurophysiol* 101: 1463–1479, 2009. First published December 17, 2008; doi:10.1152/jn.90681.2008. Responses of a visual neuron to optimally oriented stimuli can be suppressed by a superposition of another grating with a different orientation. This effect is known as cross-orientation suppression. However, it is still not clear whether the effect is intracortical in origin or a reflection of subcortical processes. To address this issue, we measured spatiotemporal responses to a plaid pattern, a superposition of two gratings, as well as to individual component gratings (optimal and mask) using a subspace reverse-correlation method. Suppression for the plaid was evaluated by comparing the response to that for the optimal grating. For component stimuli, excitatory and negative responses were defined as responses more positive and negative, respectively, than that to a blank stimulus. The suppressive effect for plaids was observed in the vast majority of neurons. However, only ~30% of neurons showed the negative response to mask-only gratings. The magnitudes of negative responses to mask-only stimuli were correlated with the degree of suppression for plaid stimuli. Comparing the latencies, we found that the suppression for the plaids starts at about the same time or slightly later than the response onset for the optimal grating and reaches its maximum at about the same time as the peak latency for the mask-only grating. Based on these results, we propose that in addition to the suppressive effect originating at the subcortical stage, delayed suppressive signals derived from the intracortical networks act on the neuron to generate cross-orientation suppression.

INTRODUCTION

Responses of simple cells are described generally well by Gabor-like linear receptive fields followed by a static nonlinearity (DeAngelis et al. 1993; Jones and Palmer 1987). Responses of complex cells are in turn characterized as the sum of the outputs such simple cells (Adelson and Bergen 1985; Heeger 1992a,b; Ohzawa et al. 1990). However, there are additional nonlinear properties that cannot be explained by these standard models. One of the well-known examples is cross-orientation suppression, where the response to an optimally oriented grating is reduced by a superposition of a second grating of a different orientation (mask) even though the second grating by itself is ineffective (Bonds 1989; DeAngelis et al. 1992; Morrone et al. 1982, 1987). A superposition of two gratings is known as a plaid (Adelson and Movshon 1982; Morrone et al. 1982), and the degree of suppression is quantified by the difference in the responses to the optimal grating and the plaid.

Historically, cross-orientation suppression has been thought to be generated by intra-cortical inhibitory networks among cortical neurons with a wide range of stimulus preferences (Albrecht and Geisler 1991; Bonds 1989; DeAngelis et al. 1992; Heeger 1992b). Based on this idea, several models have been proposed to explain the cross-orientation suppression phenomenon (Albrecht and Geisler 1991; Carandini et al. 1997; Heeger 1992a; Somers et al. 1995). The most convincing evidence in support of this notion is the finding that cross-orientation suppression was blocked by the application of the GABA antagonist bicuculline (Morrone et al. 1987). However, Freeman and his colleagues have proposed an alternative model of cross-orientation suppression that is not based on intracortical networks but on a feed-forward organization: signals from LGN are attenuated by synaptic depression at the thalamocortical synapses, i.e., just before entering cortical neurons (Carandini et al. 2002; Freeman et al. 2002). Subsequently, Priebe and Ferster (2006) and Li et al. (2006) suggested a similar but slightly different model in which the cross-orientation suppression originates from nonlinear properties, such as contrast saturation in the LGN, and the output nonlinearity in the cortex.

To elucidate the possible site or the source of the cross-orientation suppression, most previous studies have examined tuning properties of cross-orientation suppression by varying the orientation, spatial frequency, or temporal frequency of mask stimuli, thereby determining what combination of these parameters is most effective for suppression (Allison et al. 2001; Bonds 1989; DeAngelis et al. 1992; Ramoa et al. 1986). The tuning properties for the suppression were compared with the excitatory tuning characteristics of a population of neurons in the visual cortex and LGN (Allison et al. 2001; Bonds 1989; DeAngelis et al. 1992; Freeman et al. 2002; Sengpiel and Vorobyov 2005). The basic idea is that the tuning profiles for the suppression would reflect the properties of neurons from which the suppression signal originates. These studies, however, did not examine the response to mask-only gratings directly because most neurons are simply silent to mask-only stimuli even though the neurons may be hyperpolarized internally (Andersen et al. 2000; Ferster 1986; Monier et al. 2003). Some studies recorded the membrane potential of the neuron to the plaid stimuli (Berman et al. 1991; Douglas et al. 1991; Priebe and Ferster 2006).

Most of previous studies mainly focused on the spatial tuning properties for plaid patterns, and the temporal aspect of cross-orientation suppression has been ignored (but see Smith et al. 2006). In this study, we directly measured spatiotemporal response profiles of neurons to plaid patterns as well as to individual component gratings using a subspace reverse corre-

Address for reprint requests and other correspondence: I. Ohzawa, Graduate School of Frontier Biosciences and School of Engineering Science, Osaka University. 1-3 Machikaneyama, Toyonaka, Osaka 560-8531 Japan (E-mail: ohzawa@fbs.osaka-u.ac.jp).

The costs of publication of this article were defrayed in part by the payment of page charges. The article must therefore be hereby marked "*advertisement*" in accordance with 18 U.S.C. Section 1734 solely to indicate this fact.

0022-3077/09 $8.00 Copyright © 2009 The American Physiological Society

Downloaded from http://jn.physiology.org/ by 10.220.33.3 on June 24, 2017

lation method (Bredfeldt and Ringach 2002; Nishimoto et al. 2005; Ringach et al. 1997). A subspace reverse correlation method allows us to measure not only the excitatory but also suppressive responses by adding a blank stimulus in a stimulus sequences (Bredfeldt and Ringach 2002). Examining the time course of suppression would help us to understand the mechanism of cross-orientation suppression. If cross-orientation suppression was the result of intracortical networks, suppressive signal for the plaid would be delayed compared with the excitatory signals, i.e., the response to the optimal grating. On the other hand, if cross-orientation suppression were a mere reflection of sub-cortical phenomena, suppressive signal for the plaid would be received at the same time as that for the excitatory signals. In this case, the time course of response to the plaid would be similar to that for the optimal stimulus as if these responses were scaled version of each other in amplitude only. To assess these possibilities, we compared the responses to the plaid and its component grating stimuli with respect to both timing and amplitude. Furthermore, to elucidate the spatiotemporal structure for cross-orientation suppression as those shown for responses to single gratings (Malone and Ringach 2008; Mazer et al. 2002; Ringach et al. 2002), our stimulus set included a whole matrix of orientations and spatial frequencies as mask stimuli.

METHODS

All experimental procedures were performed in accordance with the National Institutes of Health Guidelines for the Care and Use of Laboratory animals and approved by the Animal Care and Use Committee of Osaka University.

Surgical procedure

Fourteen adult cats weighing 2.5–4.2 kg were prepared for single-unit recording. The animal was premedicated with subcutaneous injections of hydroxyzine hydrochloride (Atarax-P, 0.8 mg/kg) and atropine sulfate (0.02 mg/kg). Twenty minutes after the injection, anesthesia was induced by mask inhalation of 3.0–4.0% isoflurane in O_2 initially and gradually lowered and maintained at 1.5–2.5% for the remainder of the surgical preparation. A local anesthetic, lidocaine, was applied to incisions and points of pressure. Cefotiam hydrochloride (Panspolin, 5 $mg \cdot kg^{-1} \cdot day^{-1}$ im) and dexamethasone sodium phosphate (Decadron, 0.1 mg/kg im) were administered. Catheters were placed in at least two veins for drug and fluid infusion, and a glass tracheal cannula was inserted for artificial respiration. After the animal was secured in a stereotaxic apparatus, paralysis was induced with an initial dose of gallamine triethiodide (10–20 mg iv) and maintained with a continuous infusion (10 $mg \cdot kg^{-1} \cdot h^{-1}$ iv). The infusion fluid also contained sodium thiopental (Ravonal, 1 $mg \cdot kg^{-1} \cdot h^{-1}$ iv) as anesthetic and glucose (40 $mg \cdot kg^{-1} \cdot h^{-1}$) in Ringer solution. The animal was artificially ventilated with a gas mixture of 70% N_2O-30% O_2 with isoflurane (~0.5%) added as needed when the heart rate was >250~260 beat/min. Lactated Ringer solution with 5% dextrose was continuously administered through the other catheter at a rate of 2 $ml \cdot kg^{-1} \cdot h^{-1}$. During the experiment, the end-tidal CO_2 was maintained between 3.5 and 4.2% by adjusting the ventilator. Rectal temperature was monitored and maintained at 37.0–39.0° C with a thermostatically controlled heating pad. Pupils were dilated with 1% atropine sulfate, and nictitating membranes were retracted with 5% phenylephrine hydrochloride (Neosynesin) every 8–12 h. The corneas were also protected using contact lenses of appropriate power with a 3- to 4-mm artificial pupil. A craniotomy (5 × 5 mm) was performed over the area 17 or 18 (Horsley–Clarke P4 L2 for recordings of A17, A3 L3 for A18). The underlying dura was incised, and once the electrodes were positioned, the hole was covered with 5% agar in Ringer solution. Melted wax was applied over the agar to improve stability of the recordings.

Recording procedure

Neural activity was recorded using tungsten microelectrodes (5 MΩ, A-M Systems). Two electrodes were mounted in parallel in a single protective guide tube with a diameter of 1 mm and driven by a common micromanipulator (Narishige, Tokyo, Japan). The electrodes were advanced at oblique angles (10–20° anterior, and 0–10° medial) to the cortical surface and usually traversed 3–6 mm. The signals from the electrodes were amplified, band-pass filtered (200–5,000 Hz) and fed into a custom-made data-acquisition system with 40-μs time resolution. This system allowed us to discriminate spike waveforms on the basis of shape and amplitude.

Histology

At the end of experiments, the animals were administered an overdose of pentobarbital sodium (Nembutal), and perfused transcardially with buffered saline solution followed by 30% formalin in 0.1 M phosphate-buffered saline (PBS). The cortex was blocked and immersed in formalin containing a graded series of sucrose (10–30%). The blocks were frozen and sectioned into 60- to 100-μm slices and stained with thionin. To identify the location and the area of recorded cells, we reconstructed electrode tracks of the cortical slices by locating electrolytic lesions (3–7 s, 5–10 μA) with intervals of 500–1,200 μm and visualizing tissue damage from the passage of the electrode. Locations of electrode tracks were identified under a light microscope.

Visual stimulation

Visual stimuli were generated by custom software based on a Windows-based personal computer with a graphics card (Millennium G550; Matrox, Dorval, Quebec, Canada). This computer was controlled by another Windows-based computer which specified stimulus parameters for each trail. Stimuli were presented on a cathode ray tube (CRT) monitor (GDM-FW900; Sony, Tokyo, Japan) at a resolution of 1,600 × 1,024 pixels and a video frame rate of 76 Hz, with a mean luminance of 40 cd/m^2. The display was gamma-corrected with a lookup table. We placed a haploscope in front of the cat, which allowed dichoptic presentations of visual stimuli to left and right eyes separately on two halves of the display, each consisting of 800 × 1,024 pixels. The distances from the screen to the eyes were kept at 57 cm, subtending the visual field of 23(horizontal) × 30(vertical) degrees for each eye.

Experimental protocol

Once action potentials of one or more cells were isolated, we conducted a preliminary search for estimating the cells' preferred orientations and spatial frequencies, as well as the approximate positions of the receptive fields using a mouse-controlled search program. We then attempted to determine the center position of the receptive field using the minimum size of grating patch necessary for eliciting a response. Ocular dominance was also estimated at this time. Following these initial tests, the optimal orientation and spatial frequency for each cell was determined using a subspace reverse correlation mapping (Nishimoto et al. 2005; Ringach et al. 2002) and/or conventional drifting grating tests (see more detail in Sanada and Ohzawa 2006). In most cases, the receptive field of the neuron was also obtained using a standard reverse correlation

Downloaded from http://jn.physiology.org/ by 10.220.33.3 on June 24, 2017

procedure (Nishimoto et al. 2006; Sasaki and Ohzawa 2007). The stimulus size was, in general, set to 1.2–2.0 times that of the classical receptive field of the cell. For cells with strong surround suppression, the stimulus size was determined by a size tuning protocol with drifting grating stimuli. Patches of grating with optimal orientation and spatial frequency were presented about the center portion of receptive field of the cell while changing the diameter of the circular grating patch. Stimulus diameters typically ranged from 0.5 to 16.0°. The optimal size determined by the size tuning was used thereafter. These values were then used to set stimulus parameters for the rest of measurements.

After these preliminary tests, we measured temporal response profiles of neurons to plaid patterns (superposition of two gratings) as well as those to individual component gratings using a modified version of reverse-correlation method (Fig. 1*A*). The stimulus set included three kinds of gratings: optimal, mask, and plaid. These stimuli were flashed sequentially for 26 ms each in a randomized order. The order of stimuli was reshuffled for every sequence. The orientation and spatial frequency for the optimal stimuli were set to the optimal values determined as noted above. The mask orientation was varied to cover 180° in 15 or 20° steps (12 or 9 orientations), while the mask spatial frequency was varied within the range that sufficiently covered the excitatory pass-band of each neuron. Frequencies were sampled in logarithmic or linear scale (7–11 spatial frequencies). The optimal parameter for suppression is not necessarily orthogonal in orientation and similar in spatial frequency to the optimal for excitation (Nishimoto et al. 2006; Ringach et al. 2002). Therefore in previous studies in which only the orthogonal and equal-frequency mask was used, it is possible that some of the suppressive effects were missed. We wished to eliminate such a possibility by using many orientations and spatial frequencies as mask stimuli. A plaid stimulus was constructed from a superposition of two gratings: the optimal and mask grating. A set of plaids constructed in this manner are shown in Fig. 1*B* (reduced for clarity). Each plaid stimulus in Fig. 1*B* actually represents multiple stimulus conditions consisting of different combinations of phases. These phase combinations (for the plaid enclosed by a dashed square in Fig. 1*B*) are illustrated in Fig. 1*C*. For both the optimal and mask, individually as component gratings and in combination as a plaid, four spatial phases were used in multiples of 90°. Therefore the entire set of plaids consists of optimal (1 orientation × 1 spatial frequency × 4 phases) and mask (9–12 orientations × 7–11 spatial frequencies x 4 phases) stimuli for a total of 1,008–2,112 plaid stimuli that were interleaved randomly along with single component gratings and blank stimuli.

For the plaid stimulus requiring two superimposed gratings, the component gratings were displayed on alternate scan lines (line interleaving) to avoid any interaction of the two components resulting from the bandwidth limitations and nonlinearities of the video system (Walker et al. 1998). Accordingly, the component gratings (optimal and mask stimulus) were displayed on alternate scan lines, while the remaining half of the scan lines had the mean luminance. The nominal contrast of all component stimuli was always kept at 80% for individual scan lines. The actual contrast of each grating component after integration on the screen is halved and was at 40% (Walker et al. 1998). Some studies reported that an increase in contrast of the mask stimulus induces a strong effect of cross-orientation suppression (Bonds 1989; DeAngelis et al. 1992; Walker et al. 1998), and basic parameters of orientation and spatial frequency tunings of cortical neurons are independent of stimulus contrast (Sclar and Freeman 1982). However, the contrast of the component stimuli was kept at the same value because it is known that the contrast affects the time course of the responses (Albrecht 1995; Albrecht et al. 2002; Carandini and Heeger 1994; Gawne et al. 1996). This is because the central aim of this study is direct comparisons of the latencies across different stimulus conditions in the same neuron. In addition, we included a blank stimulus with the mean luminance (uniformly gray screen) among the sequence to provide a baseline measurement. A blank stimulus was interleaved four times in each sequence to provide a measure of baseline response. All stimuli were presented in a randomized order at the rate of 38 Hz, refreshed every two video frames (26 ms). Depending on the responsiveness of the neurons, stimulus sequences were re-randomized and repeated 35–100 times to obtain sufficient number of spikes and acceptable signal-to-noise ratios.

Temporal profile

Evoked spike responses and the stimulus sequence were cross-correlated to obtain time courses of response for different stimulus conditions (DeBoer and Kuyper 1968). This calculation was performed for correlation delays from −50 to 300 ms in 5-ms steps. Including a blank stimulus in the sequence allowed us to detect response enhancement and suppression with respect to the baseline (Bredfeldt and Ringach 2002). By dividing the spike counts to a given stimulus by that to the blank, we could calculate the strength of the response relative to the baseline. This transformation is needed because mask-only responses were generally small in amplitude with linear scaling. Furthermore, the log transformation of the ratio gives us a metric essentially proportional to the d' (detectability) value

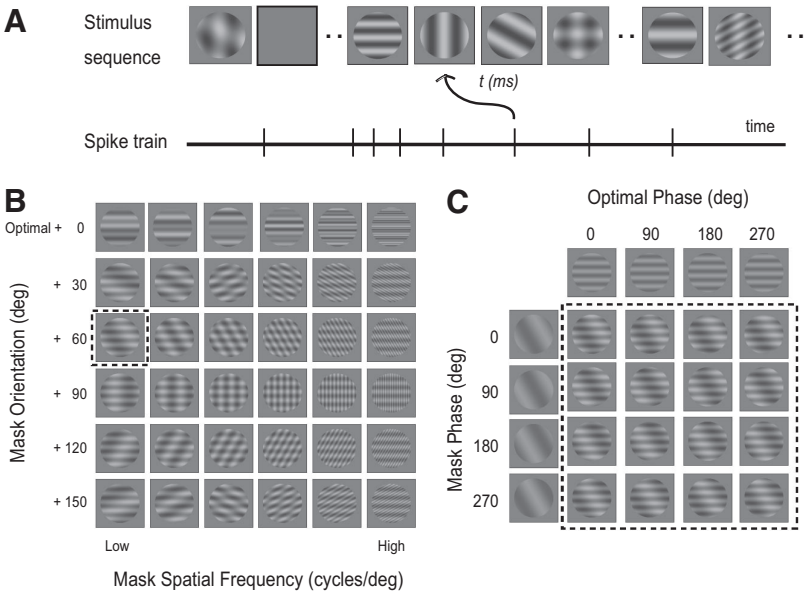

FIG. 1. Subspace reverse correlation method modified for inclusion of plaid stimuli. *A*: a stimulus sequence includes 3 kinds of gratings: the optimal, mask, and plaid. A blank stimulus is interleaved in the sequence to provide a measure of baseline response. *B*: plaid patterns in the sequence are a superposition of 2 gratings: optimal (1 orientation, 1 spatial frequency, and 4 phases) and mask gratings at different orientations, spatial frequencies and spatial phases (9 or 12 orientations, 7–11 spatial frequencies, and 4 spatial phases). Only a subset of plaid patterns is shown in *B* for clarity. *C*: all possible phase combinations (90° steps) for 1 plaid pattern (dashed rectangle in *B*) are shown (enclosed by dotted line). The *topmost row* shows the optimal gratings and the *leftmost column* shows the mask-only gratings.

Downloaded from http://jn.physiology.org/ by 10.220.33.3 on June 24, 2017

between the response and the baseline (Bredfeldt and Ringach 2002). Adopting the convention of Ringach and his colleagues, we define the response ratio as response ratio (τ) = $\log_{10}$[spike count(stimulus, τ)/spike count(blank, τ)].

Positive values indicate excitation to the stimulus at a time delay τ, whereas negative values indicate suppression. To establish an objective criterion, we used the variability of the responses at negative correlation delays, from –50 to 0 ms. Variability of the responses at negative delays should represent noise as the negative delays actually represent future relative to the times of spikes and are noncausal (Bredfeldt and Ringach 2002; Ohzawa et al. 1996). We calculated the mean ± SD of the response ratios during negative correlations delays and estimated the significance of excitation and suppression. The criterion for significance was defined as ±2 SD of the noise from the mean. If the response was above the criterion and remained above this level for a period of ≥15 ms, cells were identified as having a significant excitatory response to the stimulus. The same criterion was applied below the mean to determine the presence of a significant suppression.

RESULTS

We measured temporal response profiles of 62 orientation-selective cells in areas 17 and 18 from 14 cats (52 cells from area 17, and 10 cells from area 18). We included only those cells for which the measurement contained ≥3,000 spikes, and the maximum response amplitude to the optimal stimulus exceeded three times that of the root mean square (RMS) of the noise level. The noise level was estimated as the average response variance for negative correlation delays, from –50 to 0 ms. Cells were stimulated through the dominant eye, while the nondominant eye viewed a blank screen of equal mean luminance. For all cells included in this report, their receptive fields were located within 20° of the area centralis.

Phase dependence of temporal response profiles

The stimulus set we used (Fig. 1) was exhaustive in that we measured responses to all possible combinations of mask parameters including not only a variety of orientations and spatial frequencies but also different combinations of phases. In analyzing responses for all stimulus conditions, we must treat data from simple and complex cells somewhat differently with respect to phase due to the well-known difference in the phase sensitivity. To illustrate the point, we show temporal response profiles to plaid patterns and their individual grating components (i.e., optimal and mask gratings alone) for a representative cell of each type (Fig. 2).

Figure 2*A* shows responses from a simple cell. The matrix of temporal response profiles are arranged in the same order as that of Fig. 1*C*. In each profile, a positive value indicates that the response was enhanced for a given stimulus relative to the response to a blank stimulus. A negative value indicates that a given stimulus suppressed the response below the level produced by a blank. Because simple cells are sensitive to the spatial phase of the gratings, the responses to the optimal stimulus showed strong phase dependence as shown in the *top row*. The mask-only responses are generally insensitive to the spatial phase of the mask gratings as indicated by the *leftmost column,* where the responses are similar for all phases. The temporal responses to the plaid patterns with different combinations of optimal and mask spatial phases are shown in the rest of the panel. Because the reduction of responses for the plaid patterns was nearly constant across a given column, we selected one (or 2 if the optimal phase was straddled) column with the largest responses to the optimal stimulus as indicated by an enclosing dashed rectangle in Fig. 2*A*. The waveform traces within the rectangle were averaged for the selected plaid responses for this and other simple cells. For comparison, the temporal responses obtained in this manner for the plaid, optimal, and mask conditions are shown superimposed in Fig. 2*A, top left panel.*

Figure 2*B* presents responses from a complex cell. In contrast to simple cells, complex cells are generally insensitive to the spatial phase of gratings. The temporal responses to opti-

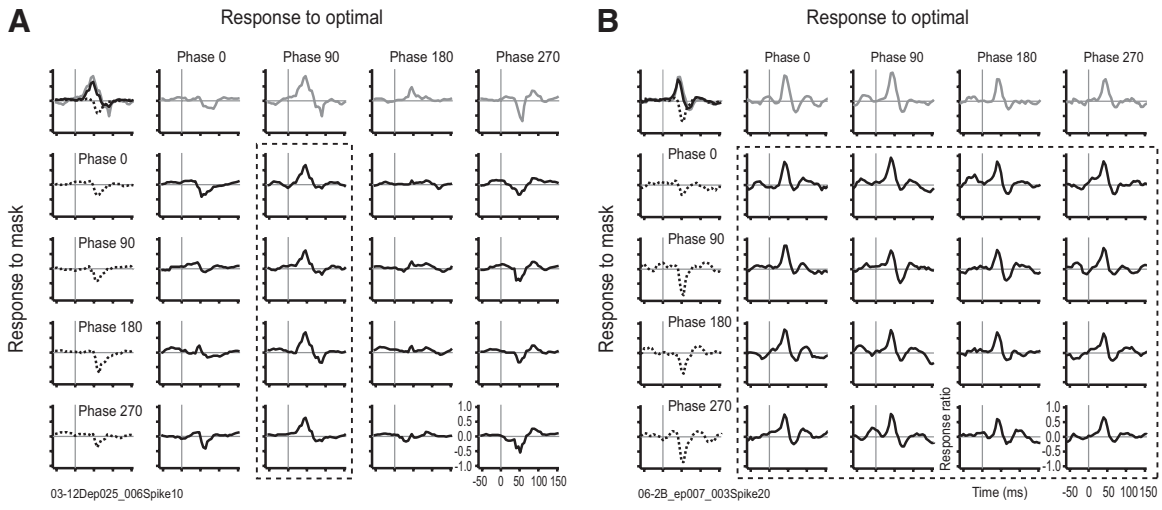

FIG. 2. Spatial phase dependence of temporal responses to plaid patterns and their component gratings. *A*: temporal response profiles for a simple cell in area 18. *B*: temporal response profiles for a complex cell in area 17. For both neurons, the *topmost row* shows temporal responses to the optimal grating of 4 different spatial phases. The *leftmost column* shows temporal responses to the mask-only stimuli, again for 4 phases. Temporal responses to plaid patterns for all possible phase combinations for the optimal and mask gratings are shown in the rest of the panel. The solid curve in the *top left corner* shows the average of temporal responses to plaids enclosed within the dashed rectangle. The gray and dashed curves in the *top left corner* depict the averaged responses to optimal gratings and mask-only gratings, respectively. The horizontal line represents the baseline activity in response to a blank stimulus. A positive value along the *y* axis indicates an excitatory effect to the stimulus, whereas a negative value indicates a suppressive effect to the stimulus at a given time delay. The response ratio is logarithmic in that 1.0 means that the response to a stimulus is 10 times larger than that to the blank.

Downloaded from http://jn.physiology.org/ by 10.220.33.3 on June 24, 2017

mal gratings were nearly identical for all four phases, and the mask-only responses were also insensitive to the spatial phases of the gratings. Due to the phase insensitivity of complex cells, responses to all the plaid stimuli with different combinations of spatial phases were similar. Therefore we averaged all the 16 waveform traces within the dashed rectangle for this and most other complex cells. Again, the temporal responses obtained in this manner for plaid, mask-only, and optimal conditions are shown superimposed in Fig. 2*B, top left.* Note, however, that some complex cells exhibited phase dependence for the responses to the optimal stimuli. We classified such a neuron as phase sensitive, if the cell fulfilled at least one of the following criteria: *1*) responses to optimal stimuli for different phases exhibited a sign inversion (detected by negative correlation values: the threshold was set to −0.2), *2*) the time of peak response for the two largest waveform traces to the optimal stimuli differed >5 ms. For such complex cells, the same analysis procedure was applied as that for simple cells. In total, we recorded from 34 simple and 28 complex cells based on the F1/F0 ratio and/or the structure of the receptive field. Of the complex cells, eight cells exhibited a phase-selective response for the optimal grating. Recent studies suggested that V1 neurons fall on a simple/complex continuum rather than two distinct classes (Mechler and Ringach 2002; Priebe et al. 2004). Therefore other than the difference in selecting the traces to average as noted in the preceding text, we did not strictly distinguish data from simple and complex cells for further analyses. In the analyses in the following text, data for these composite plots are quantified and compared across conditions.

Examples of temporal profiles

From our data set containing all possible combinations of orientation and spatial frequency of the mask stimuli, we first examine the set of responses where the maximally effective suppression was observed to the mask-only stimulus. If there is no or little suppressive effect to a series of mask-only stimuli, the condition was selected where the mask stimulus was approximately orthogonal to the optimal and the spatial frequency of the mask stimulus was as close to the optimal as possible.

Figure 3 illustrates six examples of the temporal response profiles to the plaid and its individual components for neurons recorded from areas 17 and 18. In each panel, temporal response profiles to the optimal, mask, and plaid conditions are represented by thin, gray dotted, and thick curves, respectively. We estimated the time course of suppression by subtracting the temporal response profile to the plaid pattern from that to the optimal stimulus (shaded part of Fig. 4*B*). This suppression profile is plotted as thin dotted curves in Fig. 3. In trying to account for this suppression, we initially attempted a linear prediction using the responses to component gratings. We found that a simple linear summation model was insufficient

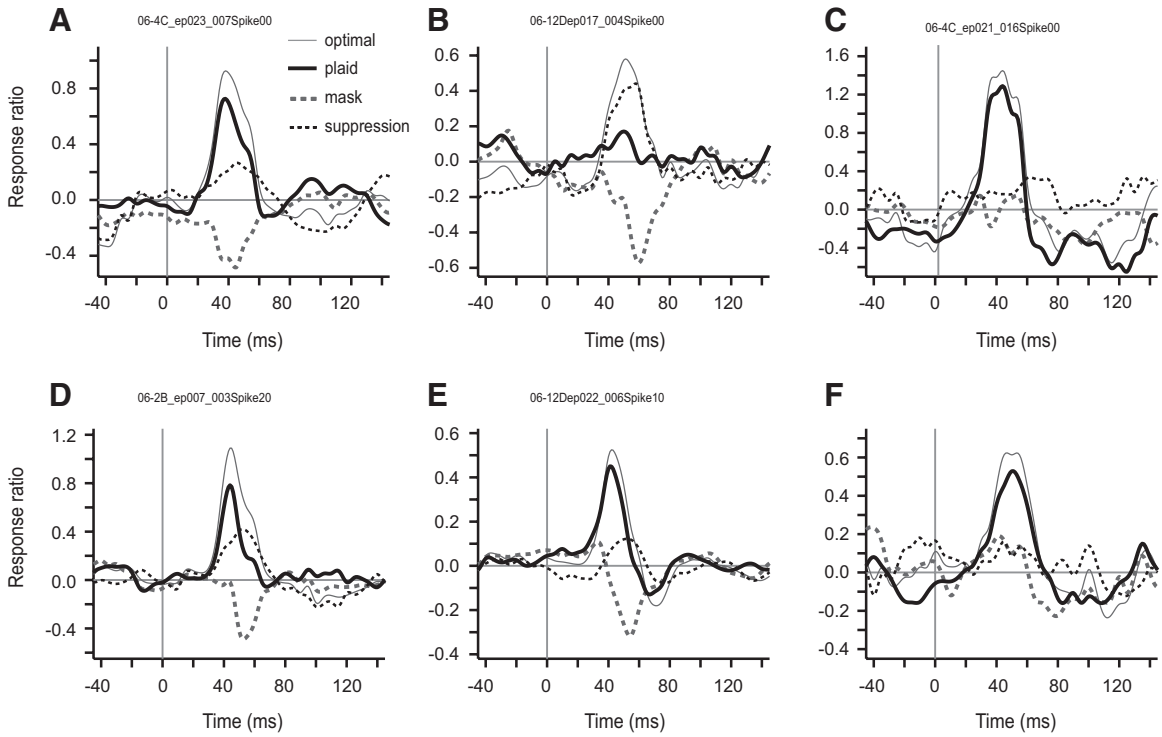

FIG. 3. Temporal responses to a plaid pattern and its component gratings for 6 representative neurons. Temporal response profiles to the optimal, mask-only, and plaid stimuli are shown by thin, gray dotted, and thick curves, respectively. The suppression time course, the difference between the optimal and the plaid responses, is also plotted by dotted curve. *A*: simple cell in area 17. The orientation and spatial frequency of the optimal stimulus is 142° and 0.22 cycle/deg, respectively. The orientation and spatial frequency of the mask stimulus is 222° and 0.18 cycle/deg, respectively. *B*: complex cell in area 17. Parameters for the optimal stimulus: 69° and 0.77 cycle/deg. Parameters for the mask stimulus: 169° and 0.65 cycle/deg. *C*: simple cell in area 18. Parameters for the optimal stimulus: 150° and 0.13 cycle/deg. Parameters for the mask stimulus: 230° and 0.12 cycle/deg. *D*: complex cell in area 17. This neuron is the same as Fig. 2*B*. Parameters for the optimal stimulus: 163° and 0.33 cycle/deg. Parameters for the mask stimulus: 243° and 0.34 cycle/deg. *E*: complex cell in area 17. Parameters for the optimal stimulus: 170° and 0.40 cycle/deg. Parameters for the mask stimulus: 250°, and 0.31 cycle/deg. *F*: simple cell in area 17. Parameters for the optimal stimulus: 210° and 0.80 cycle/deg. Parameters for the mask stimulus: 290° and 0.87 cycle/deg.

Downloaded from http://jn.physiology.org/ by 10.220.33.3 on June 24, 2017

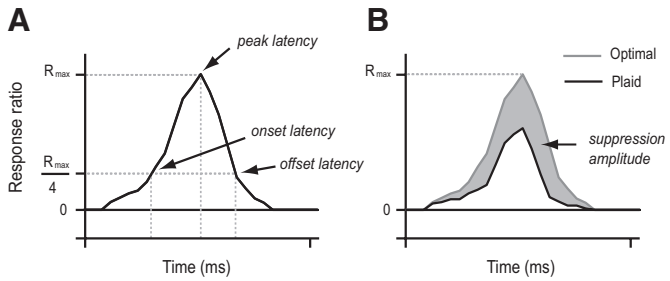

FIG. 4. Definition of the parameters to characterize a temporal response profile. *A*: the peak latency is defined as the time of the maximum or minimum response from the stimulus onset. Onset and offset latencies are defined as the time of 25% of the maximum response. *B*: suppression for the plaid pattern is estimated as the difference of the temporal responses between the optimal and the plaid.

for accounting for cross-orientation suppression. For example, the spike counts for the cell of Fig. 3*A* at the peak for the optimal, mask-only, plaid, and blank conditions are, 45, 3, 25, and 6 spikes, respectively. The difference between the optimal and plaid responses was nowhere near the amplitude of mask-only response. Hereafter, all the temporal profiles were plotted using the logarithmic scale because mask-only responses were generally small in amplitude with a linear scale (see METHODS).

Figure 3 shows that the all six neurons responded to the optimal stimulus with an increase in firing which peaks at ~30–60 ms after the stimulus onset (thin lines in Fig. 3, *A–F*). In addition, some cells showed a negative response to the mask-only stimulus at between 40 and 70 ms (gray dotted lines in Fig. 3, *A, B, D,* and *E*). In our population, ~30% of the neurons (19/62 cells) showed negative responses to some of the mask-only stimuli, and the rest of the cells did not exhibit any apparent negative response to a series of mask-only stimuli (gray dotted lines in Fig. 3, *C* and *F*). Although most cells showed positive response to plaid patterns with similar delays as those to the optimal stimuli, their responses were reduced compared with those for the optimal stimulus (thick lines in Fig. 3, *A, B, D,* and *F*). For cells with strong cross-orientation suppression (Fig. 3, *A, B,* and *D*), the peak suppression appears to be delayed with respect to the peak of the optimal response, and is actually close to that of mask-only response. Some cells exhibiting a strong negative response to the mask-only stimuli showed a completely suppressed response to the plaid patterns (Fig. 3*B*). A small number of neurons did not show any suppressive effect to the plaid patterns, meaning that the response to the plaid was almost the same as that to the optimal (Fig. 3*C*).

As noted in the preceding text, there appears to be some differences in the timing of responses to different stimuli for some neurons. For example, for the cell of Fig. 3*D,* the responses to the optimal and plaid stimuli reach their peak at ~45 ms, whereas the mask response peaks at ~55 ms. Comparing the temporal profiles among the three stimuli for each neuron, we noticed a tendency that the temporal response profiles for the plaid pattern were similar, except for scaling, to that for the optimal stimulus and that the responses to the mask stimulus were slightly delayed compared with that for the optimal and plaid stimuli. In the following sections, we quantify these qualitative observations by examining a variety of parameters describing different aspects of temporal response profiles.

Comparison of latencies between the plaid pattern and its components

To facilitate comparisons of responses to plaid and their individual components gratings across the population of cells, we introduce three temporal parameters: *peak latency*, *onset latency*, and *offset latency* (see Fig. 4*A*). These parameters have previously been used to characterize the temporal profiles of neurons (Cai et al. 1997). First, all temporal profiles were interpolated in 1-ms steps using a cubic spline function. After interpolation, *peak latency* was defined as the time of maximal or minimal point following the onset of stimulation. Having determined the peak latency, we searched backward in time from the peak for the delay at which the response first crosses <25% of the maximum response. This time was defined as the onset latency. We have also examined an alternative method to assess onset latency. The mean ± SD of the responses preceding the stimulus onset were calculated using noncausal delays (from –50 to 0 ms) to estimate the SN ratio. In this case, the onset latency was defined as the first time when the temporal response profile exceeded the mean by ≥2 SD for >10 ms (Bredfeld and Ringach 2002; Smith et al. 2006). Using temporal response profiles to the optimal stimulus condition, we compared onset latencies between these two methods. The two metrics of the latency were roughly comparable and showed significant correlation ($r = 0.8$, $n = 62$, $P < 0.05$). We have adopted the former method to estimate the onset latency in this paper. This is because the SN ratio value tended to be too sensitive to variability in offset (Fig. 3*F*) and divergence (Fig. 3*A*) during the noncausal period used (−50 to 0-ms correlation delay), causing unreasonably high values for the criterion. In some cases, weak responses such as mask-only responses were often comparable to the criterion level, thereby pushing the onset time unreasonably close to the peak latency. A similar procedure was applied to determine offset latency. For the suppression profile (shaded part of Fig. 4*B*), we also defined the three temporal parameters, *peak latency, onset latency,* and *offset latency* in the same manner.

First, we compared the peak latencies among the three stimulus conditions. Figure 5*A* compares the peak latency for the optimal and plaid stimuli for the 56 neurons that showed significant positive response to both of these stimuli. Almost all points are on or near the diagonal line, and they are strongly correlated ($r = 0.97$, $n = 56$, $P < 0.01$). The median values of the peak latency for the optimal and plaid stimulus were 45.0 and 44.0 ms, respectively. These results indicate that the response latencies for the plaid are a reflection of those for the optimal grating. Figure 5*B* compares the peak latencies between the optimal and mask-only stimuli for the 19 neurons that showed a significant negative response to the mask-only stimulus. Most of the points are above the diagonal line, indicating that the peak response for the mask-only stimulus is delayed compared with that for the optimal grating. The peak latencies for the mask (median: 54.0 ms) are longer than that for the optimal grating (median: 45.0 ms), and this difference was statistically significant ($n = 19$, $P < 0.01$, Wilcoxon signed-rank test). We also examined the relationship of the peak latencies between the plaid and mask-only conditions. The basic features are, of course, similar to the result of Fig. 5*B* (data not shown) because of similar latencies for optimal and plaid stimuli.

Downloaded from http://jn.physiology.org/ by 10.220.33.3 on June 24, 2017

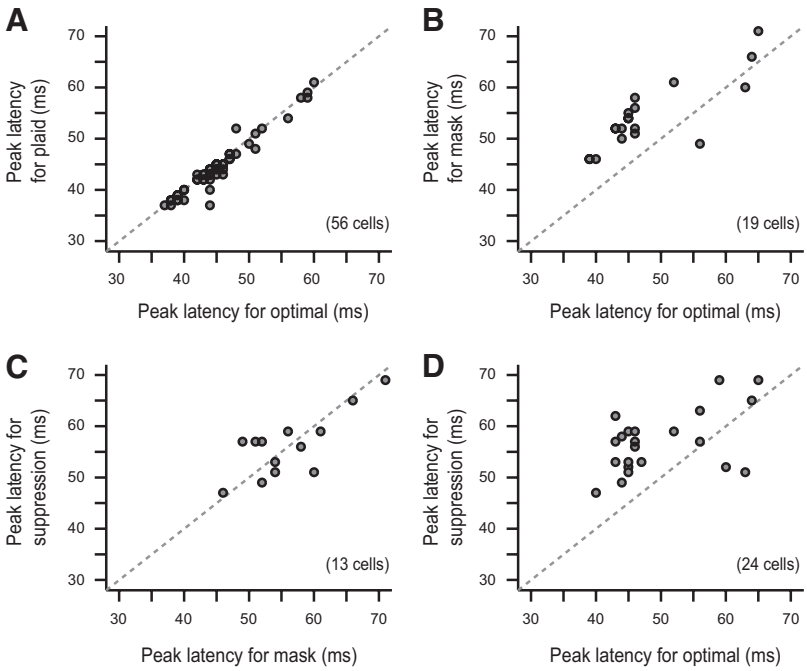

FIG. 5. Comparisons of the peak latencies for temporal responses to a plaid pattern and its components. *A*: the peak latency for a plaid pattern is plotted against that for the optimal stimulus for each cell. *B*: the peak latency for the mask-only stimulus is plotted against that for the optimal stimuli. Some of the points in this panel are exactly overlapping. *C*: the peak suppression latency for the plaid is plotted against the peak latency for the mask-only stimuli. *D*: the peak suppression latency for the plaid is plotted against the peak latency for the optimal stimuli. The numbers of cells for *B* and *C* are smaller than others because not all cells exhibited a significant negative response to the mask-only stimulus.

The primary aim of this study is to reveal the timing of suppression observed in the response to the plaid patterns and to compare them to those of the component gratings. We next compared the peak latencies for the suppression and the mask-only responses for the 13 neurons (Fig. 5*C*). If the negative response to the mask-only stimulus is the primary source of this suppression, the timing of these two types of latencies should be closely similar. As shown in Fig. 5*C,* the peak suppression latencies scatter about the similar timing of the peak latency for the mask-only stimulus for most of cells. The median values of the peak suppression latency for the plaid and the peak latency for mask-only stimuli were 57.0 and 54.0 ms, respectively. We also compared the peak suppression latencies and the peak latencies for the optimal stimulus for the 24 neurons (Fig. 5*D*). The peak suppression latencies for the plaid were longer compared with those for the optimal grating, and this difference was statistically significant ($n = 24$, $P < 0.01$, Wilcoxon signed-rank test). The main reason for the small number of cells here is that the latency of suppression cannot be defined reliably for many cells. These situations occur when the optimal grating response and plaid responses are similar, i.e., when not much suppression is observed. On the other hand, the peak latencies for the optimal and plaid responses can be defined reliably for nearly all cases.

It should be noted, however, that the response peak is not the starting point of the response. Hence it is possible that the suppression to the plaid pattern is already present before the response reaches its maximum. For this reason, we next compared the onset latencies for the suppression and those for the mask (Fig. 6*A*). Except for one cell, all points lie on or below the diagonal line. There was a tendency that the onset for the suppression (median: 35.0 ms) comes slightly earlier than those of the mask-only conditions (median: 39.0 ms), and this difference was statistically significant ($n = 13$, $P < 0.05$, Wilcoxon signed-rank test). We also compared the onset latencies for the suppression and those for the optimal (Fig. 6*B*). More than half of the cells scatter above the diagonal line, and this difference was statistically significant ($n = 21$, $P < 0.01$, Wilcoxon signed-rank test). There was not any significant difference for the response latencies between simple and complex cells.

Figure 7 summarizes the distribution of the response latencies for the plaid and its component gratings for our population of cells; white, gray, and black represent the onset, peak, and offset latency, respectively. The medians of the onset latency for the optimal, mask-only, plaid were 31.0, 39.0, and 30.0 ms, respectively. The medians of the offset latency for the optimal, mask-only, and plaid were 62.0, 74.0, and 59.0 ms, respec-

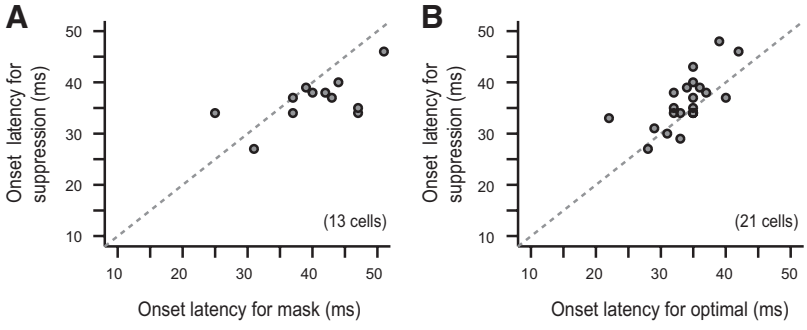

FIG. 6. Relationships between the onset latency of suppression for a plaid pattern and those for the components of the plaid. *A*: the onset latency for the suppression for a plaid is plotted against that for the mask-only stimulus for each cell. *B*: the onset latency for the suppression for the plaids is plotted against that for the optimal stimulus for each cell.

Downloaded from http://jn.physiology.org/ by 10.220.33.3 on June 24, 2017

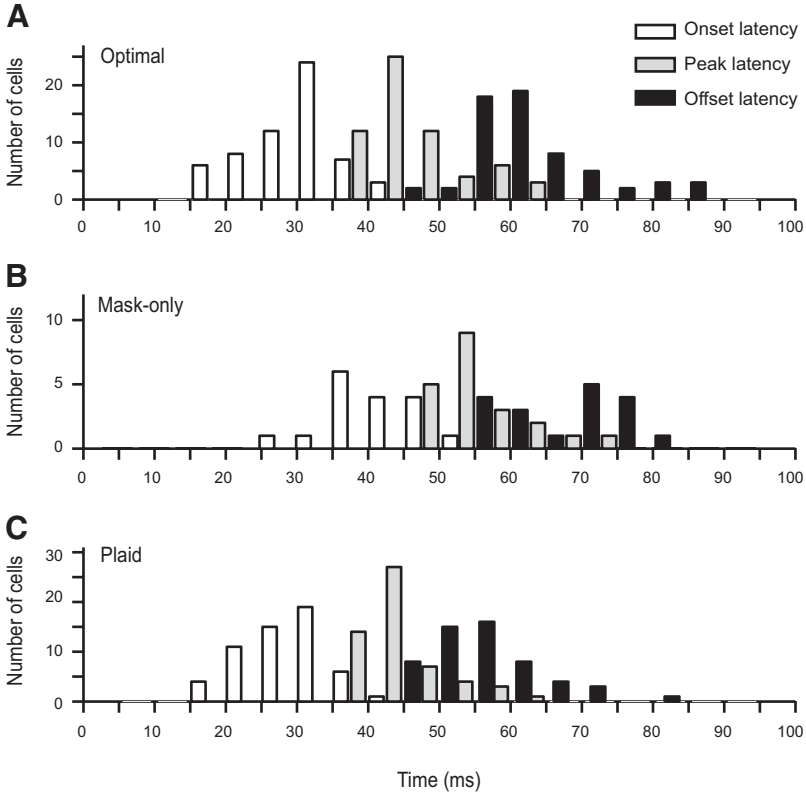

FIG. 7. Summary of the response latencies for a plaid pattern and its components in our sample of cells. *A*: distribution of the latencies for the optimal stimuli. □, ▨, and ■, the onset, peak, and offset latencies, respectively. *B*: distribution of the latencies for the mask-only stimuli that caused a significant negative response for each cell. *C*: distribution of the latencies for the plaid patterns.

tively. Comparisons of these histograms show that onset and peak for the mask-only condition (Fig. 7*B*) are delayed substantially with respect to those for the optimal and plaid conditions (Fig. 7, *A* and *C*). Interestingly, the offset latency for the plaid condition appears to be shorter than that for other conditions on average.

These results on response latencies show, in general, that suppression for the plaid pattern starts at about or slightly later than the response onset for the optimal stimulus and that the suppression for the plaid pattern reaches its maximum at about the same time as the peak response to the mask-only stimulus.

Average temporal profiles

To summarize the characteristics of temporal response profiles for our population of cells, we constructed the average temporal profiles for the optimal, mask-only, and plaid stimuli. The suppression profile, the difference between the optimal and the plaid, is also plotted as the dotted curve. To observe the effect of the negative response to the mask-only stimuli, the average temporal profiles were plotted separately based on the responses to the mask-only stimulus: one with significant negative response to the mask-only stimuli (Fig. 8*A*; 19/62, 31%), and the other without any apparent negative or positive response to the mask-only stimuli (Fig. 8*B;* 39/62, 63%). Four cells were excluded from this average profiles because mask-only stimuli elicited excitatory responses. Temporal profiles from different cells are aligned at the peak latency for the optimal stimulus and then computing the average waveforms. As shown in Fig. 8, the suppressive effect for plaid patterns was observed regardless of the presence of the negative response to the mask-only stimuli. Nevertheless, the strength of suppression is more pronounced for the cells with negative response to the mask-only stimuli. As for the timing, the averaged time courses of suppression appear to be delayed similarly for the two groups. Although the optimal grating and plaid responses appear similar by casual inspection, strictly speaking, they cannot be considered scaled versions of each other for both groups with and without mask-only responses.

Comparison of response magnitudes between the plaid pattern and its components

So far, we have concentrated on the analyses of the response latencies ignoring the response magnitude. The results of this study also allowed us to examine whether the strength of suppression for the plaid pattern was related to the magnitude

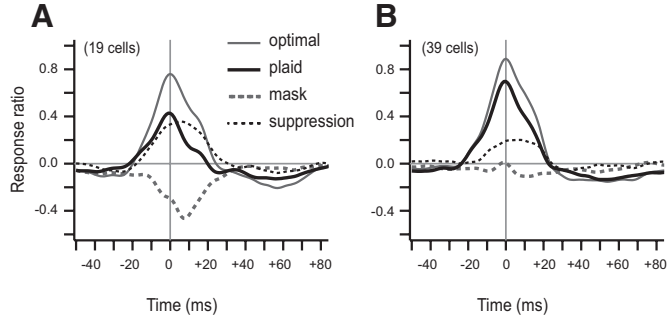

FIG. 8. Average temporal responses to a plaid pattern and its components. The suppression time course is also plotted by dotted curve. Average temporal responses are shown separately for two groups of neurons: those with (*A*) and without (*B*) a negative response to mask-only stimulus. The temporal responses from different cells were aligned at the peak latency for the optimal stimulus for each cell (vertical line) before taking the average. In both *A* and *B,* thin, gray dotted, and solid curves depict responses to the optimal, mask-only, and plaid stimuli, respectively. The suppression profile is plotted as dotted curve.

Downloaded from http://jn.physiology.org/ by 10.220.33.3 on June 24, 2017

of the responses to the component gratings. To quantify this comparison, we defined the response magnitude and the suppression strength as follows. The response magnitude for a plaid pattern and the optimal stimulus was calculated by averaging responses over the 10-ms period, 5 ms before and after the peak for the optimal stimulus. The response magnitude for the mask-only stimulus and the suppression strength was calculated during the 10 ms starting from the peak for the optimal stimulus. Therefore the time window for estimating the strength of suppression and mask-only responses included an additional delay of 5 ms relative to the optimal response. This additional delay is based on Fig. 5*B* in which the peak latency for the mask response was delayed on average by several milliseconds. Assuming that this average trend also holds for all cells, we could include in the analyses those cells for which suppression and mask-only response were weak or absent. Because the model we are trying to examine has an internal delay between the signals to be compared, it seems natural to examine the correlation between signals with the delay included.

Figure 9*A* compares the magnitude of responses to the plaid and the optimal stimuli for 58 cells without excitatory responses to mask-only stimuli. Because it is possible that the magnitude of mask-only response and the suppression strength are related, we also divided the data into two groups: cells exhibiting negative response to the mask-only stimuli (●; n = 19/62) and those without any apparent negative or positive response (×; n = 39/62). Here again, four cells were excluded from this comparison because mask-only stimuli elicited excitatory responses. For both groups, there were significant correlations between the magnitude of response to the plaid and the optimal stimulus (●; $r = 0.85$, $P < 0.01$; ×; $r = 0.81$, $P < 0.01$). For most of cells, the magnitude of response to the plaid pattern was weaker than that to the optimal grating alone, and this tendency is more pronounced for the cells with the negative response to the mask-only stimulus (Fig. 9*A*). The slopes of the regression lines were 0.85 and 0.83 for ● and ×, respectively. We also compared the magnitude of responses to the optimal and the mask-only stimuli (Fig. 9*B*). There was no significant correlation between these two values for both groups (●; $r = -0.20$, $P > 0.05$; ×; $r = -0.11$, $P > 0.05$).

It is of interest to know whether the response magnitude to mask stimulus is related to the suppression strength for the plaid pattern. We next compared the magnitude of suppression and the amplitude of mask-only responses. Figure 9*C* illustrates that the stronger the negative responses to the mask-only stimuli were, the greater were the magnitudes of suppression for the plaid pattern. There was a significant correlation between these two values ($r = -0.40$, $n = 58$, $P < 0.01$). As for the amplitude, there was a slight difference between simple and complex cells. Some neurons with weak cross-orientation suppression tended to be simple rather than complex cells. The converse was not true.

Orientation and spatial frequency dependence of cross-orientation suppression

Of the extensive amount of data, we have so far analyzed and compared the latencies and the magnitude of the responses to the plaid pattern and their components gratings for only one combination of mask orientation and spatial frequency for each cell. Many studies have shown that the strength of suppression for the plaid patterns varied depending on the orientation, spatial frequency, and temporal frequency of the superimposed mask gratings (Allison et al. 2001; Bonds 1989; DeAngelis et al. 1992; Freeman et al. 2002; Ramoa et al. 1986). Therefore we next examined the entire dataset including the orientation and spatial frequency tuning of the strength of suppression for the plaids and compared them with the responses to the component gratings.

Figure 10 illustrates an example of a complete set of temporal responses for a complex cell. The matrix of response profiles are arranged in the same order as that of Fig. 1*B*. The spatial frequency of the mask grating is constant across rows, and the orientation of the mask is constant across columns. Each panel depicts temporal response profiles for a plaid pattern and its component gratings. The temporal response to the optimal grating is identical for all plots (gray curves). The shapes and amplitudes of temporal response profiles to the mask-only stimuli changed according to the orientation and spatial frequency (dotted curves). Positive responses to mask-only stimuli are visible near the top and bottom of Fig. 10, which is expected to occur when the orientation and/or spatial frequency of the mask are close to the optimal and within the excitatory tuning bands. Negative responses to nonoptimal mask-only stimuli were present in the center portion of the

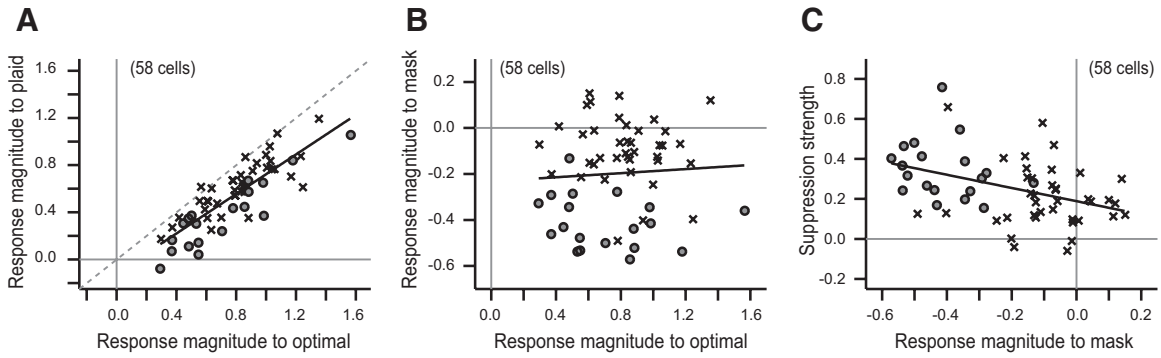

FIG. 9. Comparison of response magnitudes between a plaid and its component gratings. The data were divided into 2 groups: cells with a negative response to the mask-only stimulus (●) and those without any apparent negative or positive response (○). *A*: the magnitude of response to the plaid is plotted against that to the optimal stimulus for all neurons. *B*: the magnitude of response to the mask-only stimulus is plotted against that to the optimal stimulus. *C*: suppression strength for the plaid is plotted against the response magnitude to the mask-only stimulus. —, a linear regression line for all cells combined. The correlation coefficients are 0.84, 0.06, and −0.40, respectively.

Downloaded from http://jn.physiology.org/ by 10.220.33.3 on June 24, 2017

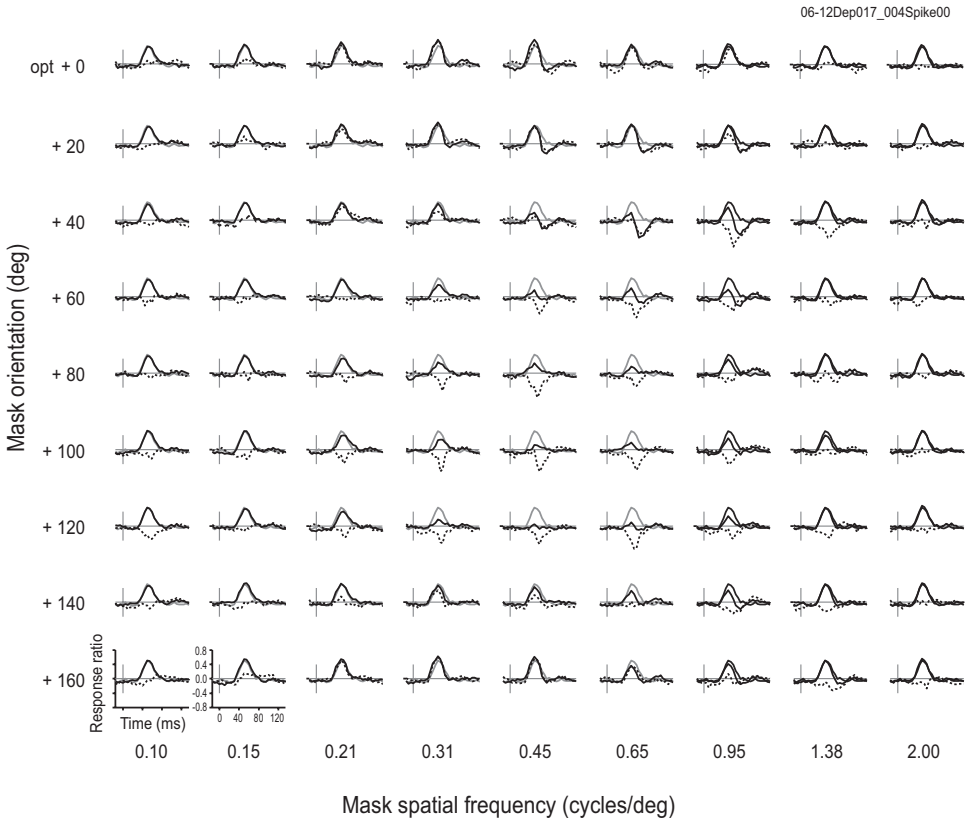

FIG. 10. A complete set of the temporal responses for a complex cell. This neuron is the same as Fig. 3*B*. The orientation of the mask stimuli is constant for a given row, and the spatial frequency of the mask stimuli is constant for a given column. Each panel depicts temporal responses to a plaid pattern and its component gratings. The temporal response to the optimal grating is identical for all plots. Responses to the optimal, mask-only and plaid stimuli are represented by gray, dotted, and solid black curves, respectively. The orientation and spatial frequency of the optimal stimulus is 69° and 0.77 cycle/deg, respectively.

figure, i.e., near the orthogonal orientation and close to the optimal spatial frequency (mask orientations: optimal +60 to +120°, mask spatial frequencies: 0.21 to 0.95 cycle/deg). Even though the responses to the mask-only stimuli showed a variety of temporal response profiles from negative, none, and to positive, the responses to the plaid (solid curves) stimuli exhibited relatively constant waveforms that were always positive and smaller in amplitude than that to the optimal stimulus (gray curves).

To visualize the dependence of suppression on mask spatial frequency, orientation, and time, the data in traces of Fig. 10 are replotted in Fig. 11*A* as spatial frequency-orientation maps at a series of time delays at 5-ms intervals from 35 to 65 ms. The plaid response minus the optimal response is shown as a density plot, each pixel representing the suppression at a given combination of spatial frequency and orientation arranged in the same way as in Fig. 10. The suppression for plaid patterns (blue) emerges at 40 ms and reaches a peak at 55 ms. The suppression was strongest near the center of the maps where the mask parameters were near the orthogonal orientation and close to the optimal spatial frequency. Figure 11*B* illustrates the responses to the mask-only gratings in the same format. Strong negative responses to the mask-only gratings (blue) were also observed near the center of the domain. The mask parameters effective for eliciting the negative responses to the mask-only stimuli tended to evoke the strong suppression to the plaid pattern as well. However, onset times for the suppression and mask-only responses were different. Mask-only responses were not visible clearly until ~50–55 ms. Positive responses (red) were also observed near the top and bottom edges of the plots in Fig. 11. These two maps showed a significant correlation ($r = 0.57$, $P < 0.01$, at 55 ms). A similar tendency was observed for two other neurons. For the cell of Fig. 11, *C* and *D,* the suppression and mask-only responses were similar in the time course as well as in the spatial frequency-orientation domain. For the cell of Fig. 11, *E* and *F,* the suppression for the plaid was present well before the onset of the negative response to the mask-only stimuli.

It is of interest to examine whether there is a specific spatiotemporal structure for cross-orientation suppression because it has been reported that the optimal spatial frequency evolves with time to a higher frequency in the case of simple single-grating excitation (Bredfeldt and Ringach 2002; Mazer et al. 2002; Nishimoto et al. 2005). Figure 12*A* illustrates the time evolution of peak spatial frequency for cross-orientation suppression for the 14 cells that showed clear spatial frequency tunings for a duration of ≥20 ms. Temporal profiles from different cells are aligned at the peak latency for the optimal stimulus for each cell (indicated as 0 ms), and the peak spatial frequency was estimated by fitting a Gaussian function to the spatial frequency tuning at each delay. The spatial frequency tuning for suppression was estimated by averaging the responses at two (or 3) orientations where the maximally effective suppression was observed at the peak delays. The range of averaging was changed depending on the tuning width for each cell. There was a general tendency that the optimal spatial frequency for suppression evolved with time to a higher frequency for most of cells, in the manner similar to the shifts found for excitation.

To quantify the rate of change in optimal spatial frequency, we calculated the shift ratio of the peak spatial frequency during the 10-ms periods, from 0 to 10 ms, for the suppression. To further compare the shift for peak spatial frequency between the suppression (blue regions in Fig. 11, *A, C,* and *E*) and

Downloaded from http://jn.physiology.org/ by 10.220.33.3 on June 24, 2017

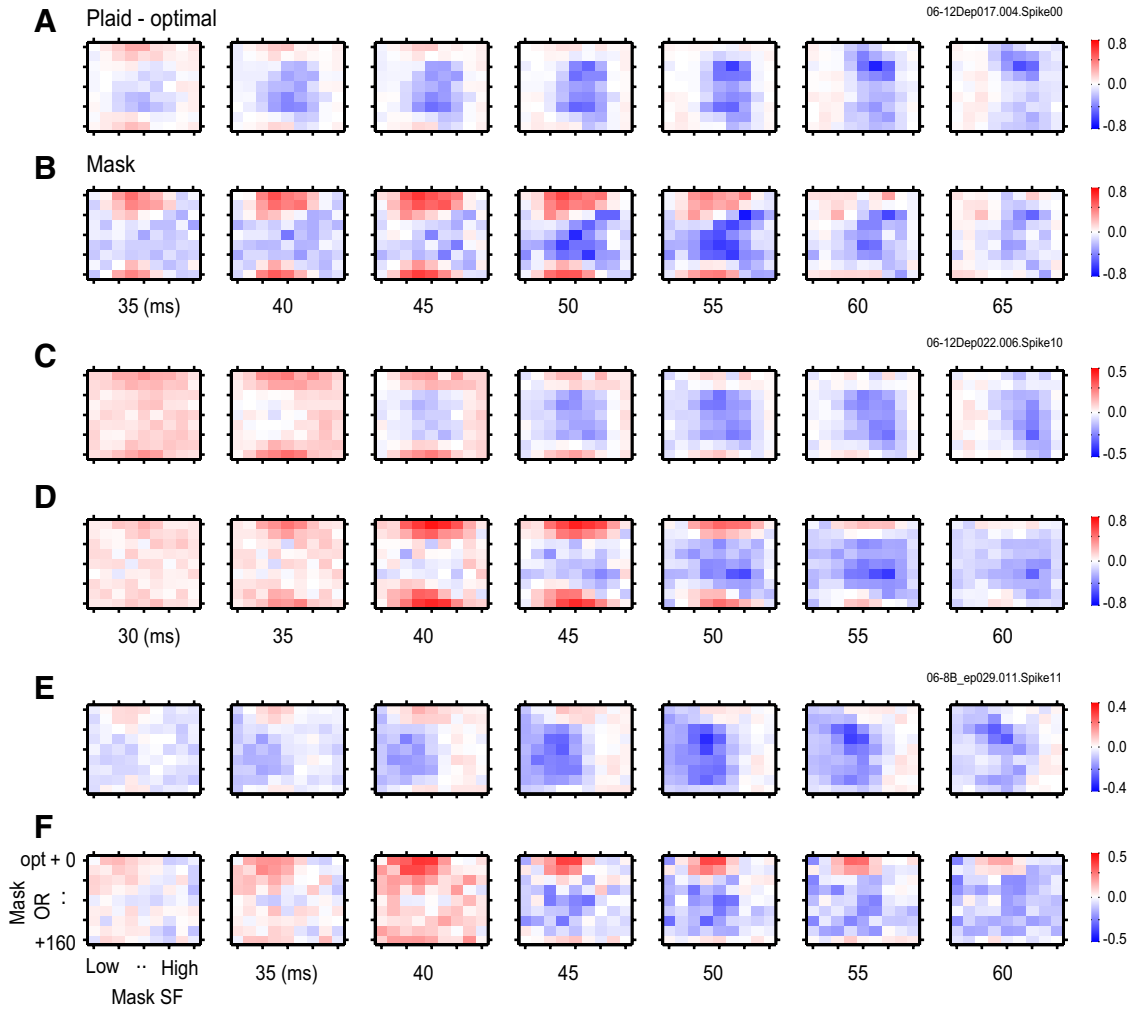

FIG. 11. Time evolution of suppression and mask-only responses in the spatial frequency-orientation domain for three representative neurons. The upper part (*A, C,* and *E*) shows suppression (plaid response - optimal response) for the plaid patterns as a function of the spatial frequency and orientation of the mask stimuli at a series of delays. Negative (blue) and positive (red) values indicate suppression and excitation, respectively. Zero (white) indicates that the response to the plaid patterns is equal to that of the optimal grating alone. The lower part (*B, D,* and *F*) shows mask-only responses in the same manner. *A* and *B*: complex cell in area 17. This neuron is the same as Figs. 3*B* and 10. The orientation and spatial frequency of the optimal stimulus is 69° and 0.77 cycle/deg, respectively. The peak latency for the optimal is 45 ms. The range of spatial frequency of the mask stimuli is 0.10–2.00 cycle/deg. *C* and *D*: complex cell in area 17. This neuron is the same as Fig. 3*E*. The orientation and spatial frequency of the optimal stimulus is 170° and 0.40 cycle/deg, respectively. The peak latency for the optimal is 40 ms. The range of spatial frequency of the mask stimuli is 0.08–1.20 cycle/deg. *E* and *F*: complex cell in area 17. The orientation and spatial frequency of the optimal stimulus is 265° and 0.30 cycle/deg, respectively. The peak latency for the optimal is 40 ms. The range of spatial frequency of the mask stimuli is 0.08–1.20 cycle/deg.

the excitation (red regions in Fig. 11, *B, D,* and *F*), the shift ratio was also estimated for excitation in a similar manner. The excitatory tuning for single gratings was estimated by averaging two (or 3) mask-only responses around the optimal orientation. Figure 12*B* shows the result of this comparison. The shift ratio for suppression tended to be greater than that for

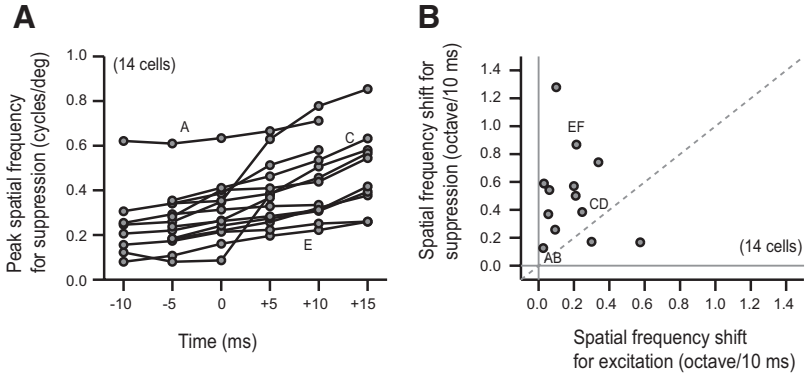

FIG. 12. Comparison of the time evolution of peak spatial frequency for cross-orientation suppression and excitation to single gratings. *A*: the change of peak spatial frequency for cross-orientation suppression as a function of time for 14 cells. Each curve indicates a change of peak spatial frequency for each cell. The data from different cells were aligned depending on the peak latency for the optimal stimulus. The peak latency is indicated as 0 ms. *B*: comparison of the shift ratios of the peak spatial frequencies for suppression and single-grating excitation during the 10-ms periods after the peak delay. Data from cells presented in Fig. 11 are depicted by their respective alphabets.

Downloaded from http://jn.physiology.org/ by 10.220.33.3 on June 24, 2017

excitation. However, some cells with peak shift for excitation does not show the shift for suppression and vice versa.

Are there specific relationships between spatial tuning parameters such as the optimal spatial frequency and bandwidth for suppression and excitation? To address this, we summarized the comparison of spatial frequency tuning curves for cross-orientation suppression, the positive and negative responses for single gratings. The *peak* and *bandwidth* were estimated by fitting a Gaussian function to the spatial frequency tuning. Because some of cells in our sample show low-pass tuning for spatial frequency, we used the *quality factor* (Bredfeld and Ringach 2002) instead of the traditional bandwidth metric (half-width at half-height in octaves). The quality factor is defined as the ratio of the optimal frequency to the difference between the high and low cutoff frequencies

$$Q = \frac{SF_{peak}}{SF_{high} - SF_{low}}$$

where SF_{high} and SF_{low} are the spatial frequencies at which the response falls to one half of the peak value. Cells with a large Q-factor show sharp spatial frequency tunings, whereas cells with a small Q-factor exhibit broad ones.

Figure 13 shows the comparisons of the peak spatial frequencies (*A–C*) and the Q-factors (*D–F*) for the 14 neurons that showed the selectivity in spatial frequency domain. Figure 13*A* compares the peak spatial frequency between the optimal and the nonoptimal mask stimuli. There is a correlation ($r = 0.53$, $n = 14$) but no clear tendency between these two values. The medians of the peak spatial frequency for the optimal and nonoptimal gratings were 0.40 cycle/deg (ranging from 0.23 to 0.58) and 0.43 cycle/deg (ranging from 0.19 to 0.64), respectively. Figure 13*B* compares the peak spatial frequency between the optimal gratings and the suppression for the plaid. Most of the points are on or below the diagonal line, indicating that the effective spatial frequency for inducing the suppression for plaids tended to be lower than that for the single grating condition. The median of the peak spatial frequency for the plaids was 0.32 cycle/deg (ranging from 0.18 to 0.63). Figure 13*C* compares the peak spatial frequency between the nonoptimal gratings and the suppression for the plaid. This result indicates that the effective spatial frequency for inducing the suppression for plaids tended to be lower than that for the nonoptimal single gratings. Similar analysis was applied to the Q-factor for the 14 cells. Figure 13*D* shows the result of a comparison of the Q-factor between the optimal and the nonoptimal gratings. Except for two cells, all points lie below the diagonal line, indicating that the suppressive tuning to nonoptimal mask-only stimuli was broader than that for the excitatory response to the optimally oriented gratings. The medians of the Q-factor for the optimal and nonoptimal gratings were 1.13 (ranging from 0.83 to 1.47) and 0.77 (ranging from 0.35 to 1.46), respectively. Figure 13*E* compares the Q-factors between the optimal gratings and the plaid conditions. This result indicates that the suppressive tuning to plaid was broader than that for the excitatory response to the optimally oriented gratings. Figure 13*F* compares the Q-factors between the nonoptimal gratings and the plaid conditions. There was no significant relationship between these values. The median of

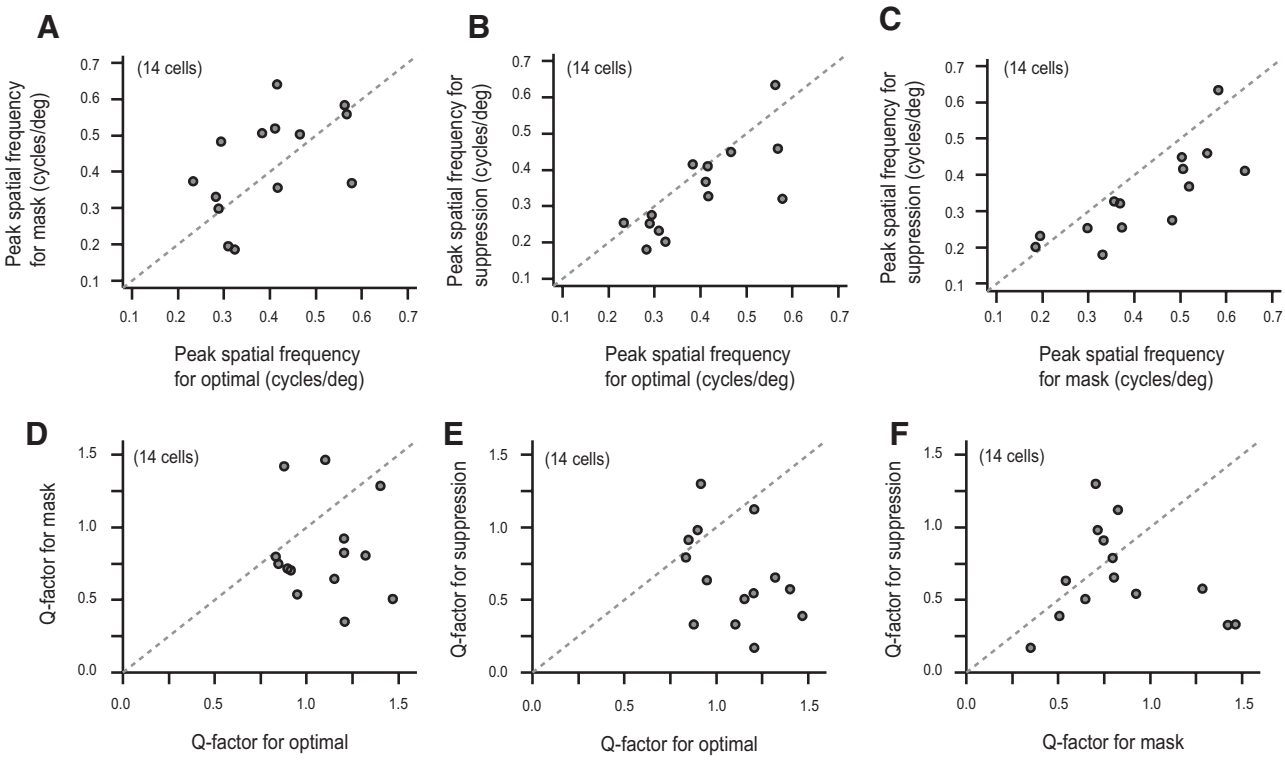

FIG. 13. Summary of spatial frequency parameters for suppression, mask-only, and optimal responses. *A*: the peak spatial frequency for the negative response to the nonoptimal mask-only grating is plotted against that for the optimal stimuli. *B*: the peak suppressive spatial frequency for the plaid is plotted against that for the optimal stimuli. *C*: the peak suppressive spatial frequency for the plaid is plotted against that for the mask-only stimuli. *D*: Q-factor for the nonoptimal mask-only grating is plotted against that for the optimal stimuli. *E*: Q-factor for the plaids is plotted against that for the optimal stimuli. *F*: Q-factor for the plaids is plotted against that for the mask-only stimuli.

Downloaded from http://jn.physiology.org/ by 10.220.33.3 on June 24, 2017

the Q-factor for the suppression was 0.72 (ranging from 0.18 to 0.63).

The orientation tuning was also estimated by examining the vertical cross-sections of Fig. 11. Figure 11 showed that the orientation tuning for suppression (blue regions in *A, C,* and *E*) is broader than that for excitation (red regions in *B, D,* and *F*). In addition, the range of orientation exhibiting suppression appears somewhat wider than the suppression with a single grating like shown in Fig. 11, *E* and *F*. In general, the dependence of response suppression on the orientation of mask gratings was weak compared with the spatial frequency as has already mentioned in DeAngelis et al. (1992). Unlike spatial frequency tunings for which we provide a summary as Fig. 13, we do not present a similar summary for orientation. This is because we could not estimate the *peak* and *bandwidth* for suppression because the orientation tuning for suppression is generally too broad and flat to define a peak reliably.

Relationships between negative responses to mask-only stimuli and the basic characteristics of neurons

We have reported that the suppression for plaid patterns was present in most of the cells, but the negative response to mask-only grating was not always present. Are there any apparent differences between cells with and without the negative response? To explore this possibility, we examined possible correlations of the presence of the negative response to other characteristics of the neurons.

Numerous studies have shown that direction selectivity is reduced by the application of bicuculline (Sillito 1977; Tsumoto et al. 1979), thus we first examined the relationship between the presence of negative responses and the direction selectivity. To characterize the direction selectivity of a cell, we defined the direction selectivity index (DSI) according to the formula DSI = 1 - (R_{np}/R_p), where R_p, R_{np} are responses to the drifting gratings with the preferred direction and nonpreferred direction, respectively (Petersen et al. 2006). The orientations are determined by the peak values of the best-fitting Gaussian functions to the orientation/direction tuning curve. Values of the DSI range from 0 (identical response to both directions) to 1.0 (no response to nonpreferred direction). The median of the DSI for the cells with negative response was 0.68 ($n = 19$), which was not significantly different from that for the other cells, 0.60 ($n = 34$) ($P > 0.05$, Mann-Whitney *U* test).

Next, we examined whether the negative responses were correlated with the presence of surround suppression. For a subset of neurons, the strength of surround suppression was estimated using stimulus-size tuning curve. The suppression strength was defined as a suppression index (SI): SI = 1 - R_{large}/R_{opt}, where R_{opt} is the maximum response, and R_{large} is the asymptotic response to large grating stimuli (Cavanaugh et al. 2002a). No significant difference was found in the median values of SI with and without the presence of negative responses to mask-only gratings ($P > 0.05$, Mann-Whitney *U* test). Obviously, the lack of correlation was not unexpected because the most effective stimuli orientation for surround suppression is generally the same as the optimal orientation for the classical receptive field (Cavanaugh et al. 2002a,b), whereas the cross-orientation suppression is present for nearly all orientations and most effective for nonoptimal orientations (DeAngelis et al. 1992).

We also examined possible dependence of the degree of suppression on binocularity, and the cortical areas, 17 and 18. There were no obvious trends with respect to these properties.

DISCUSSION

In this study, we have characterized the time course of cross-orientation suppression by comparing spatiotemporal responses to a plaid pattern and its component gratings. Spatiotemporal responses to different stimuli were measured using a subspace reverse correlation method (Bredfeldt and Ringach 2002; Nishimoto et al. 2005; Ringach et al. 1997). In what follows, we will discuss possible neural mechanisms for the origins of cross-orientation suppression, and compare our results with those of previous studies. We will also consider potential problems with our methods.

Possible origins of cross-orientation suppression

A simple idea to explain the cross-orientation suppression is a linear combination of the responses to component gratings: the positive response to the optimal and the negative response to the nonoptimal mask grating (Malone and Ringach 2008; Ringach et al. 2002). When optimal and mask gratings are presented together as a plaid, the negative response may cancel part of the excitation by the optimal stimulus, thereby reducing the overall response. If this is the case, a neuron with suppression for the plaid should exhibit negative response to mask-only stimulus. This was not always the case in our study. In addition, the averaged time courses of suppression appear to be delayed similarly for the two groups (Fig. 8). The difference between the optimal and plaid responses was nowhere near the amplitude of mask-only response. We concluded that a simple linear summation model is insufficient for accounting for cross-orientation suppression.

It is plausible that a gain control operating on a fast time scale rapidly reduce the response to plaid because the effective contrast for the plaid is increased compared with single gratings (Bonds 1991; Heeger 1992a). By definition, such a gain control added to the main linear signal pathway makes the system nonlinear as a whole. Only when the gain control is slow compared with the rate of stimulus changes as in slow contrast adaptation (Ohzawa et al. 1982), can we think of the whole system as essentially linear. Although we do not specifically address the system at that level of detail, the fast gain controls may be a possible underlying mechanism that is responsible for cross-orientation suppression.

Historically, cross-orientation suppression was interpreted as evidence for intracortically generated inhibition (Allison et al. 2001; Bonds 1989; DeAngelis et al. 1992; Morrone et al. 1982; Sengpiel and Vorobyov 2005; Sengpiel et al. 1998) because anatomical (Garey and Powell 1971; Montero 1990) and physiological (Creutzfeld and Ito 1968; Tanaka 1983) studies showed that most LGN afferents to cortex are excitatory. Recent studies, however, have challenged this notion and propose that the suppression is already present at the subcortical stage (i.e., in the LGN), and the cortical effects are mere reflections of the subcortical phenomena (Carandini et al. 2002; Freeman et al. 2002). Note that these are not necessarily mutually exclusive.

Downloaded from http://jn.physiology.org/ by 10.220.33.3 on June 24, 2017

Based on our results and those of others, we first consider the possibility of intracortical origin of cross-orientation suppression. We assume that the negative response to the mask-only stimuli is mainly derived from the intracortical networks involving inhibitory inter-neurons. Although the response decrease for the plaid could be explained by feed-forward model (Carandini et al. 2002; Freeman et al. 2002), the negative response for the mask-only grating would be difficult to account for based only on the strict feed-forward model. If cross-orientation suppression is a result of intracortically generated inhibition, suppressive signal for plaid would be delayed compared with the excitatory signals. This is because the negative signals generated via inhibitory inter-neurons go through extra steps in the cortex and therefore are delayed compared with the excitatory signals. As shown in Fig. 5*B,* the negative response to the nonoptimally oriented mask-only stimulus comes later than the positive response to the optimal stimulus (see also Malone and Ringach 2008). In addition, the peak suppression for the plaid is delayed compared with the peak latency for the optimal grating stimulus (Fig. 5*D*). Furthermore, the suppression for the plaid reaches its maximum at about the same time as the peak response to the mask-only stimulus (Fig. 5*C*). These findings are consistent with the idea that the grating of a nonoptimal orientation generates a delayed negative signal intracortically, which is then subtracted from the direct excitatory input.

There are other lines of evidence in support of the intracortical origin of cross-orientation suppression. One is a pharmacological study indicating that blocking GABA receptors in cortex removes cross-orientation suppression (Morrone et al. 1987). Another is the presence of a dichoptic form of cross-orientation suppression, termed interocular suppression (Endo et al. 2000; Li et al. 2005; Sengpiel and Blakemore 1994; Sengpiel and Vorobyov 2005; Walker et al. 1998). Binocular interactions are already present in LGN (Xue et al. 1987), but Sengpiel and Vorobyov (2005) demonstrated that interocular suppression in V1 neurons was greatly reduced by the application of the GABA antagonist bicuculline into the cortical tissue near the neuron.

Despite the lines of evidence as noted in the preceding text, some of our results could not be fully explained based only on the intracortical networks. First, the indication of cross-orientation suppression was present for most cells, but the negative response to mask-only gratings did not always occur. This finding suggests that it is necessary to consider additional factors to explain cross-orientation suppression phenomenon. Although the presence of mask-only negative response is taken as strong evidence for intracortical input, the opposite is not necessarily true. As has been already mentioned (Freeman et al. 2002), one possibility is a suppressive effect of subcortical origin, i.e., some nonlinear interaction at the level of the LGN. Reduced gain for excitatory signals from LGN outputs may explain the cross-orientation suppression without the negative responses to mask-only stimuli. In support of this notion, the shape of temporal response profiles for the plaid was similar to that for the optimal stimulus as if the plaid response was simply scaled down in amplitude. As for the timing, the peak latency for the plaids is closely similar to that for the optimal stimuli (Fig. 5*A*). In addition, we found that the suppression for the plaid is already present before the onset of the negative response to the mask-only stimuli (Fig. 6*A*). Therefore the result suggests that there may be other sources of suppression for the plaids, which are different from that for the negative response to mask-only stimuli.

Freeman et al. (2002) also claimed that the cross-orientation suppression is not of cortical origin but represent synaptic depression at the thalamo-cortical synapses. They demonstrated that the suppression is essentially immune to visual adaptation and is engaged by gratings drifting faster than 20 Hz, which exceeds the temporal resolution of most cells in primary visual cortex. They also predicted that cross-orientation suppression occurs at the beginning of the response to the optimal grating using a feed-forward synaptic depression model (see Fig. 5A in Carandini et al. 2002).

Alternatively, it is possible that the cross-orientation suppression, at least partly, is due to feedback from high-order visual areas. Allison et al. (2001) suggested a possible extrastriate origin (area 18) for the suppression based on the fact that cross-orientation suppression occurred even with high temporal frequency gratings, exceeding the normal range of temporal frequencies for exciting area 17 neurons. We recorded from areas 17 and 18, but we could not find out any noticeable difference between the areas. Considering the results of the timing of cross-orientation suppression, it is unlikely that feedback signals from high-order visual areas are primarily responsible for cross-orientation suppression.

Taken together, we conclude that, in addition to the suppressive effect originating at the sub-cortical stage, delayed suppressive signals derived from the intracortical networks act on the neuron to suppress the response to plaid pattern. This interpretation is consistent with all of the results with respect to the properties of cross-orientation suppression.

Smith et al. (2006) reaches a similar conclusion concerning the origins of cross-orientation suppression. They showed that the onset of cross-orientation suppression is fast and appears to act on the neuron even before the response onset for the optimal stimulus. They also showed that the offset of cross-orientation suppression has a greater delay than the offset of response to the optimal stimulus. Based on these results, they suggest that only the excitatory feed-forward model predicts that these two offsets have the same latency.

Priebe and Ferster (2006) suggested an alternative model in which the cross-orientation suppression originates from the nonlinear properties, such as spike rectification, contrast saturation in the LGN, and the output nonlinearity in the cortex. Their hypothesis is based on the findings that *1*) the plaid stimulus caused a decrease, rather than enhancement, of the inhibitory conductance for the cell along with the reduction of excitatory conductance, *2*) the suppression of the spike output of simple cells was almost twice the suppression of their synaptic inputs. Later, Li et al. (2006) studied the time course of recovery from cross-orientation suppression and reached a conclusion similar to that of Priebe and his colleagues. They found that the recovery time course is inconsistent with typical temporal properties of synaptic depression (Abbott et al. 1997; Chance et al. 1998; Varela et al. 1997, 1999). These previous results provide evidence that at least some of the properties of cross-orientation suppression appear to be generated subcortically. However, these models are not explicitly ruling out additional possible contributions from other sources including intracortical networks as we examined in this study. Therefore

Downloaded from http://jn.physiology.org/ by 10.220.33.3 on June 24, 2017

the previous findings do not contradict our results and interpretations on the origins of cross-orientation suppression.

Proportions of neurons with negative responses to mask-only stimuli

Ringach et al. (2002) reported that about half of neurons in monkey V1 showed response enhancement and suppression at different locations in the Fourier domain using a subspace reverse correlation method (presenting sinusoidal gratings at different orientations, spatial frequencies, and spatial phases). Their experiment and the control subset of our measurement, mask-only responses, are equivalent in that both are single grating reverse correlation. Therefore the suppressions from these two measurements may be compared. Interestingly, the negative responses to mask-only gratings were present only for 30% of the neurons we have recorded in the cat visual cortex. One possibility for this difference is signal-to-noise ratio. Because negative response is defined as a reduction of response from a baseline level, the baseline estimate must be relatively reliable for demonstrating a weak suppression, requiring a sufficiently large number of spikes. We collected on average 18,546 spikes, ranging from 3,021 to 191,223 spikes. It is possible that recordings in Ringach et al. (2002) contained more spikes than ours or were from more responsive neurons. However, we cannot verify if such differences exist as the relevant information is not available.

Other electrophysiological studies, using spike-triggered covariance (STC) analysis, demonstrated that the suppression is more prevalent in monkey V1 than in cat area 17 (Chen et al. 2007; Rust et al. 2005; Touryan et al. 2002, 2005). Using localized spectral analyses, Nishimoto et al. (2006) also reported that $<10\%$ of cells showed significant suppressive profiles in cat areas 17 and 18. Although most of the properties of neurons in cat area 17 and macaque V1 are known to be similar and inhibitory inter-neurons are common features of cortical circuits, we cannot rule out the possibility that the effective suppressions differ between cats and monkeys.

Possible consequences of biases in the stimuli

Our stimulus set unavoidably included a bias. The grating of optimal orientation and spatial frequency always appeared in all plaid stimuli, whereas gratings of other nonoptimal conditions occurred very infrequently for a given condition. We have considered possible consequences of this bias in the stimuli.

First, because the optimal stimulus was presented many more times than other stimuli, the most likely effect would be an adaptation and resulting reduction of the response amplitude (or excitatory drive) to the optimal stimulus (Ohzawa et al. 1982). In nearly all analyses conducted in this study, we always measured the degree of suppression relative to the control response level to the optimal grating. Therefore even if the adaptation reduced the excitatory drive, that reduction would apply equally to all stimulus conditions. The overall response to the optimal grating would be reduced, but the suppression would still be visible as further reduction from that adapted optimal response level. For this reason, nearly all results in this study are still valid even in the presence of the possible adaptation effect produced by the high probability of appearance for the optimal stimulus. The problem might be expected to occur when comparing responses to single-grating stimuli: the optimal and the mask-only stimuli. In this case, the response to the optimal would be decreased, but mask-only stimulus response would not be. For amplitudes, the only relevant figures are Fig. 9, *B* and *C*. Even in these cases, however, the possible adaptation effect would manifest itself as the scaling down of the horizontal axis for Fig. 9*B* and the vertical axis for *C*. Therefore the intended analyses based on these figures, i.e., examining correlations would still be valid for these cases as well.

Second, let us examine the possible effect of this adaptation on the time course of responses. In general, responses to high-contrast stimuli are known to be faster or more compressed in time than those to low-contrast stimuli (Albrecht et al. 2002; Carandini and Heeger 1994; Sclar et al. 1989). Unfortunately, to the best of our knowledge, it is not known if responses to a constant contrast are sped up as a result of adaptation. Note that we always used a fixed contrast for the optimal stimulus (as well as for the mask), and never a high (or low) contrast adapting stimuli. Therefore the only adapting effect, if any, would be due to the bias in the total duration of presentation. In the absence of definite results on this point, the likely outcome would be either time course is not affected as long as the stimulus contrast remains constant or adaptation due to longer total time of presentation causes compression of the response time course. The first case would not cause a problem. If the second is the case, the effect of adaptation would tend to cause overestimation of the difference in latencies between the optimal grating and mask-only responses by shorting the optimal response latency. However, it is clear that there definitely is a true difference in latencies between the optimal and mask-only responses because previous reverse correlation studies with unbiased single grating stimuli also found such a difference (Malone and Ringach 2008). Taken together, we believe that essentially all of the results in this study would still be valid even in the presence of adaptation effect.

ACKNOWLEDGMENTS

We thank Drs. Ichiro Fujita, Taishin Nomura, and Hiromichi Sato for valuable discussions and suggestions. We also thank laboratory members, H. Tanaka, S. Nishimoto, T. Sanada, K. Sasaki, M. Fukui, T. Ninomiya, T. Ishida, Y. Asada, Y. Tabuchi, and T. Arai for help in experiments and extensive discussions.

GRANTS

This work was supported by Ministry of Education, Culture, Sports, Science and Technology Grant 18020017, by 21st Century and Global COE Programs from Japan Society for the Promotion of Science, and by CREST Yoshioka Project of Japan Science and Technology Agency.

REFERENCES

Abbott LF, Varela JA, Sen K, Nelson SB. Synaptic depression and cortical gain control. *Science* 275: 220–4, 1997.

Adelson EH, Movshon JA. Spatiotemporal energy models for the perception of motion. *Nature* 300: 523–5, 1982.

Adelson EH, Bergen JR. Spatiotemporal energy models for the perception of motion. *J Opt Soc Am A* 2: 284–299, 1985.

Albrecht DG. Visual cortex neurons in monkey and cat: effect of contrast on the spatial and temporal phase transfer functions. *Vis Neurosci* 12: 1191–1210, 1995.

Albrecht DG, Geisler WS. Motion selectivity and the contrast-response function of simple cells in the visual cortex. *Vis Neurosci* 7: 531–546, 1991.

Downloaded from http://jn.physiology.org/ by 10.220.33.3 on June 24, 2017

Albrecht DG, Geisler WS, Frazor RA, Crane AM. Visual cortex neurons of monkeys and cats: temporal dynamics of the contrast response function. *J Neurophysiol* 88: 888–913, 2002.

Allison JD, Smith KR, Bonds AB. Temporal-frequency tuning of cross-orientation suppression in the cat striate cortex. *Vis Neurosci* 18: 941–948, 2001.

Anderson JS, Carandini M, Ferster D. Orientation tuning of input conductance, excitation, and inhibition in cat primary visual cortex. *J Neurophysiol* 84: 909–926, 2000.

Berman NJ, Douglas RJ, Martin KA, Whitteridge D. Mechanisms of inhibition in cat visual cortex. *J Physiol* 440: 697–722, 1991.

Bonds AB. Role of inhibition in the specification of orientation selectivity of cells in the cat striate cortex. *Vis Neurosci* 2: 41–55, 1989.

Bonds AB. Temporal dynamics of contrast gain in single cells of the cat striate cortex. *Vis Neurosci* 6: 239–55, 1991.

Bredfeldt CE, Ringach DL. Dynamics of spatial frequency tuning in macaque V1. *J Neurosci* 22: 1976–1984, 2002.

Cai D, DeAngelis GC, Freeman RD. Spatiotemporal receptive field organization in the lateral geniculate nucleus of cats and kittens. *J Neurophysiol* 78: 1045–1061, 1997.

Carandini M, Heeger DJ. Summation and division by neurons in primate visual cortex. *Science* 264: 1333–1336, 1994.

Carandini M, Heeger DJ, Movshon JA. Linearity and normalization in simple cells of the macaque primary visual cortex. *J Neurosci* 17: 8621–8644, 1997.

Carandini M, Heeger DJ, Senn W. A synaptic explanation of suppression in visual cortex. *J Neurosci* 22: 10053–10065, 2002.

Cavanaugh JR, Bair W, Movshon JA. Nature and interaction of signals from the receptive field center and surround in macaque V1 neurons. *J Neurophysiol* 88: 2530–2546, 2002a.

Cavanaugh JR, Bair W, Movshon JA. Selectivity and spatial distribution of signals from the receptive field surround in macaque V1 neurons. *J Neurophysiol* 88: 2547–2556, 2002b.

Chance FS, Nelson SB, Abbott LF. Synaptic depression and the temporal response characteristics of V1 cells. *J Neurosci* 18: 4785–4799, 1998.

Chen X, Han F, Poo MM, Dan Y. Excitatory and suppressive receptive field subunits in awake monkey primary visual cortex (V1). *Proc Natl Acad Sci USA* 104: 19120–19125, 2007.

Creutzfeldt O, Ito M. Functional synaptic organization of primary visual cortex neurones in the cat. *Exp Brain Res* 6: 324–352, 1968.

DeAngelis GC, Ohzawa I, Freeman RD. Spatiotemporal organization of simple-cell receptive fields in the cat's striate cortex. II. Linearity of temporal and spatial summation. *J Neurophysiol* 69: 1118–1135, 1993.

DeAngelis GC, Robson JG, Ozhawa I, Freeman RD. Organization of suppression in receptive fields of neurons in cat visual cortex. *J Neurophysiol* 68: 144–163, 1992.

De Boer R, Kuyper P. Triggered correlation. *IEEE Trans Biomed Eng* 15: 169–179, 1968.

Douglas RJ, Martin KA, Whitteridge D. An intracellular analysis of the visual responses of neurons in cat visual cortex. *J Physiol* 440: 659–696, 1991.

Endo M, Kaas JH, Jain N, Smith EL 3rd, Chino Y. Binocular cross-orientation suppression in the primary visual cortex (V1) of infant rhesus monkeys. *Invest Ophthalmol Vis Sci* 41: 4022–4031, 2000.

Ferster D. Orientation selectivity of synaptic potentials in neurons of cat primary visual cortex. *J Neurosci* 6: 1284–1301, 1986.

Freeman TC, Durand S, Kiper DC, Carandini M. Suppression without inhibition in visual cortex. *Neuron* 35: 759–771, 2002.

Garey LJ, Powell TP. An experimental study of the termination of the lateral geniculo-cortical pathway in the cat and monkey. *Proc R Soc Lond B Biol Sci* 179: 41–63, 1971.

Gawne TJ, Kjaer TW, Richmond BJ. Latency: another potential code for feature binding in striate cortex. *J Neurophysiol* 76: 1356–1360, 1996.

Heeger DJ. Normalization of cell responses in cat striate cortex. *Vis Neurosci* 9: 181–197, 1992a.

Heeger DJ. Half-squaring in responses of cat striate cells. *Vis Neurosci* 9: 427–443, 1992b.

Jones JP, Palmer LA. The two-dimensional spatial structure of simple receptive fields in cat striate cortex. *J Neurophysiol* 58: 1187–1211, 1987.

Li B, Peterson MR, Thompson JK, Duong T, Freeman RD. Cross-orientation suppression: monoptic and dichoptic mechanisms are different. *J Neurophysiol* 94: 1645–1650, 2005.

Li B, Thompson JK, Duong T, Peterson MR, Freeman RD. Origins of cross-orientation suppression in the visual cortex. *J Neurophysiol* 96: 1755–1764, 2006.

Malone BJ, Ringach DL. Dynamics of tuning in the Fourier domain. *J Neurophysiol* 100: 239–248, 2008.

Mazer JA, Vinje WE, McDermott J, Schiller PH, Gallant JL. Spatial frequency and orientation tuning dynamics in area V1. *Proc Natl Acad Sci USA* 99: 1645–1650, 2002.

Mechler F, Ringach DL. On the classification of simple and complex cells. *Vision Res* 42: 1017–1033, 2002.

Monier C, Chavane F, Baudot P, Graham LJ, Frégnac Y. Orientation and direction selectivity of synaptic inputs in visual cortical neurons: a diversity of combinations produces spike tuning. *Neuron* 7: 63–80, 2003.

Montero VM. Quantitative immunogold analysis reveals high glutamate levels in synaptic terminals of retino-geniculate, cortico-geniculate, and geniculo-cortical axons in the cat. *Vis Neurosci* 4: 437–443, 1990.

Morrone MC, Burr DC, Maffei L. Functional implications of cross-orientation inhibition of cortical visual cells. I. Neurophysiological evidence. *Proc R Soc Lond B Biol Sci* 216: 335–354, 1982.

Morrone MC, Burr DC, Speed HD. Cross-orientation inhibition in cat is GABA mediated. *Exp Brain Res* 67: 635–644, 1987.

Nishimoto S, Arai M, Ohzawa I. Accuracy of subspace mapping of spatiotemporal frequency domain visual receptive fields. *J Neurophysiol* 93: 3524–3536, 2005.

Nishimoto S, Ishida T, Ohzawa I. Receptive field properties of neurons in the early visual cortex revealed by local spectral reverse correlation. *J Neurosci* 26: 3269–3280, 2006.

Ohzawa I, DeAngelis GC, Freeman RD. Stereoscopic depth discrimination in the visual cortex: neurons ideally suited as disparity detectors. *Science* 249: 1037–1041, 1990.

Ohzawa I, DeAngelis GC, Freeman RD. Encoding of binocular disparity by simple cells in the cat's visual cortex. *J Neurophysiol* 75: 1779–1805, 1996.

Ohzawa I, Sclar G, Freeman RD. Contrast gain control in the cat visual cortex. *Nature* 298: 266–268, 1982.

Peterson MR, Li B, Freeman RD. Direction selectivity of neurons in the striate cortex increases as stimulus contrast is decreased. *J Neurophysiol* 95: 2705–2712, 2006.

Priebe NJ, Ferster D. Mechanisms underlying cross-orientation suppression in cat visual cortex. *Nat Neurosci* 9: 552–961, 2006.

Priebe NJ, Mechler F, Carandini M, Ferster D. The contribution of spike threshold to the dichotomy of cortical simple and complex cells. *Nat Neurosci* 7: 1113–1122, 2004.

Ramoa AS, Shadlen M, Skottun BC, Freeman RD. A comparison of inhibition in orientation and spatial frequency selectivity of cat visual cortex. *Nature* 321: 237–239, 1986.

Ringach DL, Bredfeldt CE, Shapley RM, Hawken MJ. Suppression of neural responses to nonoptimal stimuli correlates with tuning selectivity in macaque V1. *J Neurophysiol* 87: 1018–1017, 2002.

Ringach DL, Sapiro G, Shapley R. A subspace reverse-correlation technique for the study of visual neurons. *Vision Res* 37: 2455–2464, 1997.

Rust NC, Schwartz O, Movshon JA, Simoncelli EP. Spatiotemporal elements of macaque v1 receptive fields. *Neuron* 46: 945–956, 2005.

Sasaki KS, Ohzawa I. Internal spatial organization of receptive fields of complex cells in the early visual cortex. *J Neurophysiol* 98: 1194–1212, 2007.

Sanada TM, Ohzawa I. Encoding of three-dimensional surface slant in cat visual areas 17 and 18. *J Neurophysiol* 95: 2768–2786, 2006.

Sclar G, Freeman RD. Orientation selectivity in the cat's striate cortex is invariant with stimulus contrast. *Exp Brain Res* 46: 457–461, 1982.

Sclar G, Lennie P, DePriest DD. Contrast adaptation in striate cortex of macaque. *Vision Res* 29: 747–755, 1989.

Sengpiel F, Blakemore C. Interocular control of neuronal responsiveness in cat visual cortex. *Nature* 368: 847–850, 1994.

Sengpiel F, Baddeley RJ, Freeman TC, Harrad R, Blakemore C. Different mechanisms underlie three inhibitory phenomena in cat area 17. *Vision Res* 38: 2067–2080, 1998.

Sengpiel F, Vorobyov V. Intracortical origins of interocular suppression in the visual cortex. *J Neurosci* 25: 6394–6400, 2005.

Sillito AM. Inhibitory processes underlying the directional specificity of simple, complex and hypercomplex cells in the cat's visual cortex. *J Physiol* 271: 699–720, 1977.

Smith MA, Bair W, Movshon JA. Dynamics of suppression in macaque primary visual cortex. *J Neurosci* 26: 4826–4834, 2006.

Downloaded from http://jn.physiology.org/ by 10.220.33.3 on June 24, 2017

Somers DC, Nelson SB, Sur M. An emergent model of orientation selectivity in cat visual cortical simple cells. *J Neurosci* 15: 5448–5465, 1995.

Tanaka K. Cross-correlation analysis of geniculostriate neuronal relationships in cats. *J Neurophysiol* 49: 1303–1318, 1983.

Touryan J, Felsen G, Dan Y. Spatial structure of complex cell receptive fields measured with natural images. *Neuron* 45: 781–791, 2005.

Touryan J, Lau B, Dan Y. Isolation of relevant visual features from random stimuli for cortical complex cells. *J Neurosci* 22: 10811–10818, 2002.

Tsumoto T, Eckart W, Creutzfeldt OD. Modification of orientation sensitivity of cat visual cortex neurons by removal of GABA-mediated inhibition. *Exp Brain Res* 34: 351–363, 1979.

Varela JA, Sen K, Gibson J, Fost J, Abbott LF, Nelson SB. A quantitative description of short-term plasticity at excitatory synapses in layer 2/3 of rat primary visual cortex. *J Neurosci* 17: 7926–7940, 1997.

Varela JA, Song S, Turrigiano GG, Nelson SB. Differential depression at excitatory and inhibitory synapses in visual cortex. *J Neurosci* 19: 4293–42304, 1999.

Walker GA, Ohzawa I, Freeman RD. Binocular cross-orientation suppression in the cat's striate cortex. *J Neurophysiol* 79: 227–239, 1998.

Xue JT, Ramoa AS, Carney T, Freeman RD. Binocular interaction in the dorsal lateral geniculate nucleus of the cat. *Exp Brain Res* 68: 305–310, 1987.

Downloaded from http://jn.physiology.org/ by 10.220.33.3 on June 24, 2017